

# Learning More from Less: Unlocking Internal Representations for Benchmark Compression

Yueqi Zhang <sup>\*1</sup> Jin Hu <sup>\*1</sup> Shaoxiong Feng <sup>2</sup> Peiwen Yuan <sup>1</sup> Xinglin Wang <sup>1</sup> Yiwei Li <sup>1</sup> Jiayi Shi <sup>1</sup> Chuyi Tan <sup>1</sup>  
 Ji Zhang <sup>1</sup> Boyuan Pan <sup>2</sup> Yao Hu <sup>2</sup> Kan Li <sup>1</sup>

## Abstract

The prohibitive cost of evaluating Large Language Models (LLMs) necessitates efficient alternatives to full-scale benchmarking. Prevalent approaches address this by identifying a small coresset of items to approximate full-benchmark performance. However, existing methods must estimate a reliable item profile from response patterns across many source models, which becomes statistically unstable when the source pool is small. This dependency is particularly limiting for newly released benchmarks with minimal historical evaluation data. We argue that discrete correctness labels are a lossy view of the model’s decision process and fail to capture information encoded in hidden states. To address this, we introduce REP-CORE, which aligns heterogeneous hidden states into a unified latent space to construct representative coresets. Using these subsets for performance extrapolation, REP-CORE achieves precise estimation accuracy with as few as ten source models. Experiments on five benchmarks and over 200 models show consistent gains over output-based baselines in ranking correlation and estimation accuracy. Spectral analysis further indicates that the aligned representations contain separable components reflecting broad response tendencies and task-specific reasoning patterns.

## 1. Introduction

Large Language Models (LLMs) have demonstrated strong capabilities across diverse domains and reshaped modern AI research (Achiam et al., 2023; Dubey et al., 2024; Yang et al., 2025; Marjanović et al., 2025). Benchmark suites have therefore expanded in size, often reaching tens of thou-

<sup>1</sup>School of Computer Science, Beijing Institute of Technology <sup>2</sup>Xiaohongshu Inc. Correspondence to: Kan Li <likan@bit.edu.cn>, Shaoxiong Feng <shaoxiongfeng2023@gmail.com>.

Preprint. February 3, 2026.

sands of items, as the community continually adds new tasks and test cases while preserving comparability over time. However, full-scale evaluation at this scale incurs substantial computational and financial costs, making frequent re-evaluation impractical during rapid model iteration (Liang et al., 2022; Perlitz et al., 2024). Consequently, recent work on *benchmark compression* selects a small coresset and evaluates models on this subset to approximate full-benchmark scores and rankings (Vivek et al., 2024; Polo et al., 2024; Yuan et al., 2025).

These methods largely share the same pipeline. They first collect output-level responses from many source models on the full benchmark, forming a model-by-item matrix of correctness or confidence. Each item is then represented by its response vector across models or by low-dimensional factors estimated from this matrix, for example through Item Response Theory, and these representations support both coreset selection and score extrapolation. This pipeline implicitly assumes broad source coverage. When only a handful of source models are available, as is often the case for newly released or long-tail benchmarks with limited historical evaluations, these output-derived item representations are estimated unreliably. As a result, the geometric structure of the item space collapses and many distinct items become indistinguishable, as shown in Figure 1, leading to less representative coresets and larger extrapolation errors.

Motivated by this limitation, we investigate the internal representations produced during inference. Unlike discrete output labels, hidden states provide a high-dimensional and continuous view of the computation that generates an answer. Prior work has shown that these states encode rich internal features of uncertainty, problem difficulty, and task-dependent reasoning patterns (Azaria & Mitchell, 2023; Zou et al., 2023; Zhang et al., 2025; Orgad et al., 2024; Wang et al., 2025a). We hypothesize that hidden states offer a dense signal for characterizing items, but exploiting this signal requires aligning heterogeneous hidden spaces across architectures. To this end, we introduce REP-CORE, a framework that aligns heterogeneous hidden states into a unified latent space to recover fine-grained item structures.

REP-CORE utilizes a shared projection mechanism to map

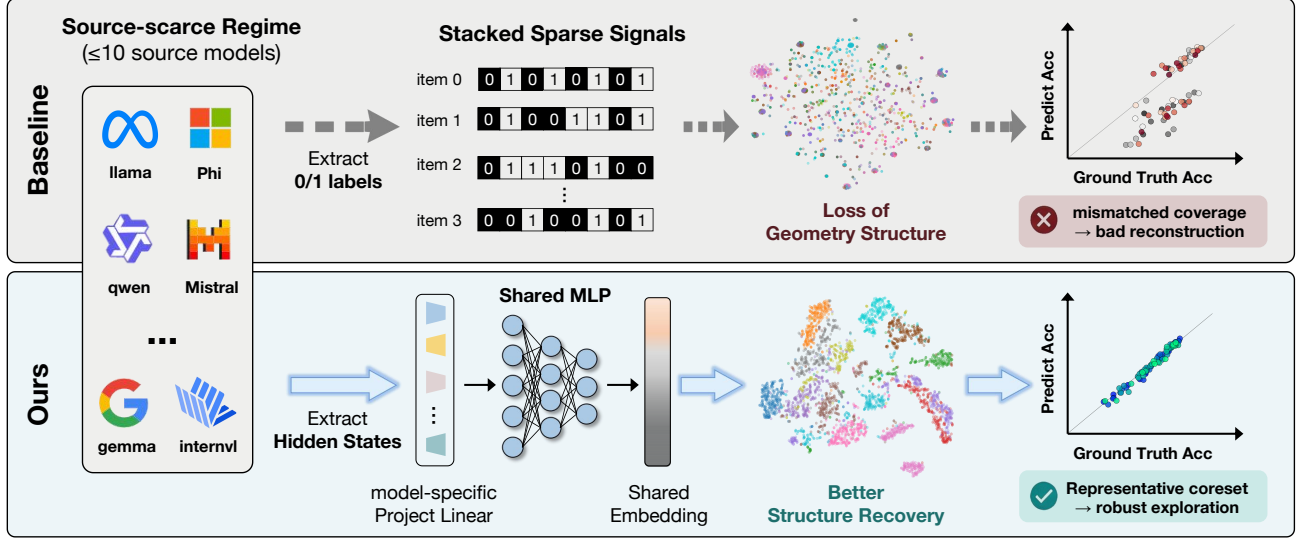


Figure 1. Comparison of item representation paradigms in source-scarce regimes. Top: Output-based methods rely on sparse 0/1 signals that fail to preserve the geometric structure of the item space. Bottom: REP CORE aligns heterogeneous hidden states into a unified latent space to recover fine-grained item structures for robust coresset selection.

model-specific hidden states into aligned embeddings, recovering the geometric structure of the item space. As shown in the bottom panel of Figure 1, aggregating these embeddings across source models reveals structured clusters associated with distinct reasoning patterns. Within this aggregated space, we employ a clustering-based strategy to select a diverse set of anchor items that serve as the training basis for a lightweight linear regressor. By extrapolating the target model’s performance from these anchors, our approach yields accurate full-benchmark estimates and remains effective even with as few as ten source models.

We conduct experiments on five benchmarks spanning text-only and multimodal settings, using over two hundred models that include text-only and multimodal variants and cover both dense and mixture-of-experts architectures. Under matched coresset sizes with ten source models, our method consistently improves full-benchmark estimation accuracy and ranking consistency over competitive output-based baselines. Our contributions are summarized as follows, with related work deferred to Appendix A:

- We formalize benchmark compression under source scarcity and show that sparse output-level signals distort the geometry of the item space, degrading both coresset selection and performance extrapolation.
- We propose REP CORE, which maps model-specific hidden states into aligned embeddings and uses the resulting space to enable robust coresset selection and accurate extrapolation with few source models.
- We provide empirical and structural evidence supporting

internal representations. Our results demonstrate that the aligned embeddings contain separable components that reflect broad response tendencies and task-specific reasoning patterns.

## 2. RepCore Approach

We propose REP CORE, a framework designed to achieve high-fidelity benchmark compression in source-scarce regimes. As illustrated in Figure 2, the pipeline operates in three consecutive phases. First, we learn aligned representations from model hidden states to recover the benchmark’s geometric structure (§2.2). Second, we perform consensus clustering in this latent space to construct a representative coresset (§2.3). Finally, we employ a lightweight and robust extrapolator to map local coresset evaluations to full-benchmark performance estimations (§2.4).

### 2.1. Problem Setup

Let  $\mathcal{I}$  denote the comprehensive set of items in a benchmark. We consider a set of available source models  $\mathcal{S}$  and a set of unseen target models  $\mathcal{T}$ , operating specifically within a source-scarce regime where  $|\mathcal{S}|$  is strictly limited. We adopt the standard *free-generation then binary-scoring* paradigm, where each source model  $m \in \mathcal{S}$  generates a response for item  $i \in \mathcal{I}$  that is deterministically parsed to yield a binary correctness label  $y_{m,i} \in \{0, 1\}$ . Concurrently, we extract the hidden state  $h_{m,i}$  associated with the generation. Our objective is to learn item representations that capture the relational structure of the benchmark, thereby guiding the selection of a minimal coresset  $\mathcal{C} \subset \mathcal{I}$ . By evaluating target

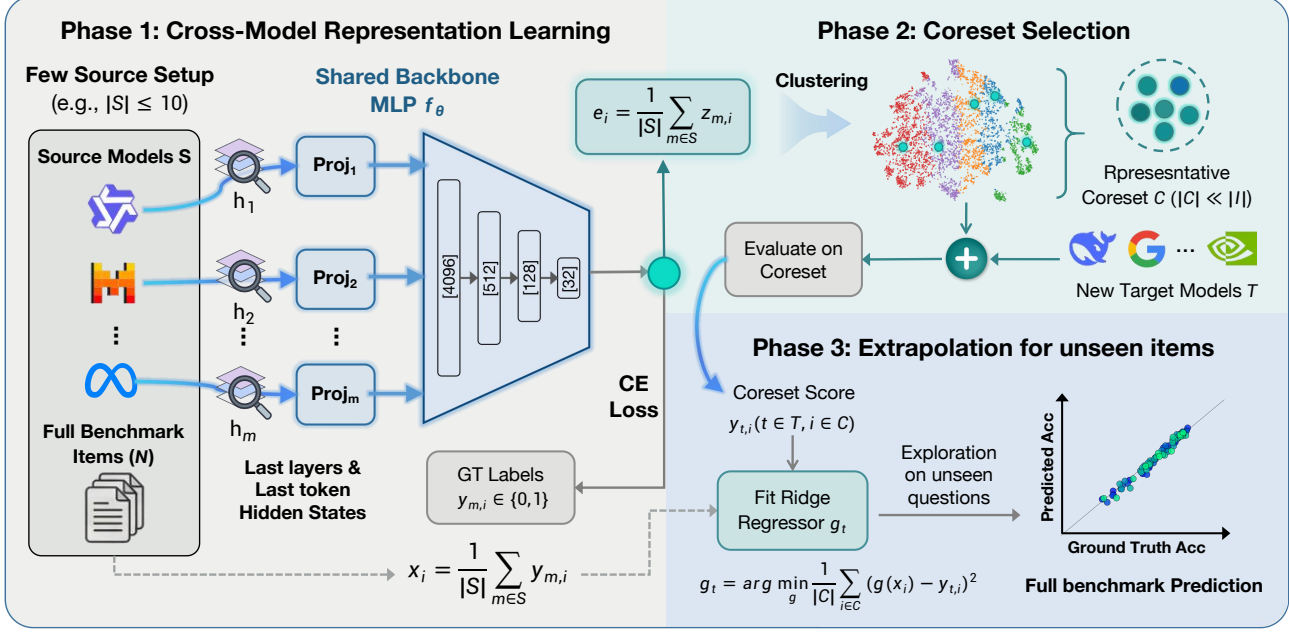


Figure 2. Overview of the REPCORE framework. The pipeline proceeds in three phases: aligning heterogeneous hidden states into a unified latent space via model-specific projections and a shared MLP, selecting representative anchor items through consensus clustering, and extrapolating full-benchmark performance using a lightweight regressor.

models exclusively on  $\mathcal{C}$ , we aim to accurately estimate their performance on the full set  $\mathcal{I}$ .

## 2.2. Cross-Model Representation Learning

Under the source-scarce regime (specifically  $|\mathcal{S}| \leq 10$ ), the response matrix  $Y$  has only  $|\mathcal{S}|$  rows and provides a highly limited view of inter-item relations. This scarcity makes inter-item relations unreliable and fails to recover the benchmark’s latent relational structure. Moreover, when the source pool is dominated by a single model family or a narrow range of model behavior, the learned space can inherit systematic biases from the sources. To mitigate this effect, we construct  $\mathcal{S}$  to span diverse model families and behaviors, and then leverage continuous hidden states to learn dense item representations.

**Hidden State Extraction** For each model-item pair  $(m, i)$ , we extract the final layer’s hidden state of the final output token, denoted as  $h_{m,i}$ . Validated by recent interpretability studies, these states encode the reasoning trajectory and decision signals, providing a high-fidelity information source superior to discrete correctness labels.

**Cross-Model Alignment and Supervision** Source models exhibit significant architectural heterogeneity, possessing distinct hidden dimensions and feature spaces. To obtain comparable representations across models without introducing systematic bias, we apply an independent linear projection layer  $\text{Proj}_m$  to each source model, followed by

a source-agnostic Multi-Layer Perceptron (MLP)  $f_\theta$ . This pipeline acts as an information bottleneck, progressively compressing the high-dimensional input into an aligned representation:

$$z_{m,i} = f_\theta(\text{Proj}_m(h_{m,i})) \in \mathbb{R}^{d_z} \quad (1)$$

We refer to  $z_{m,i}$  as the aligned embedding of item  $i$  under source model  $m$ . The dimension  $d_z$  determines the bottleneck capacity. We set  $d_z = 32$  for all subsequent experiments, as we empirically observe that for most models, the effective rank of the aligned embedding matrix (capturing 99% variance) remains below 20. Thus, 32 dimensions provide ample capacity to maintain representational richness while ensuring computational efficiency.

To explicitly extract signals directly tied to the final evaluation outcome, we apply a linear classifier  $g_\phi$  to  $z_{m,i}$  and optimize the entire network using Cross-Entropy loss to predict the ground-truth correctness  $y_{m,i}$ :

$$\mathcal{L} = \sum_{m \in \mathcal{S}} \sum_{i \in \mathcal{I}_{\text{train}}} \text{CE}(g_\phi(z_{m,i}), y_{m,i}) \quad (2)$$

We define  $\mathcal{I}_{\text{train}}$  by randomly partitioning the target benchmark  $\mathcal{I}$  into training, validation, and test splits using 70%, 10%, and 20% splits, respectively. This process treats the optimization as a representation learning task on the target distribution. Empirically, the classifier achieves high Area Under the Curve (AUC) scores peaking at approximately 0.9 on held-out test splits, confirming that the bottleneck features successfully distill validity signals. For the subsequent clustering phase, we utilize the MLP output  $z_{m,i}$ ,

as this aligned representation preserves richer information about the intrinsic relational structure of the full benchmark.

### 2.3. Coreset Selection via Consensus Clustering

To synthesize a stable structural prior from the aligned representations, we compute the consensus embedding  $e_i$  by averaging  $z_{m,i}$  across all source models. We use this consensus embedding as the item representation for coreset selection. Subsequently, we apply  $L_2$ -normalization to project the aggregated vectors onto a unit hypersphere:

$$\tilde{e}_i = \frac{e_i}{\|e_i\|_2}, \quad \text{where } e_i = \frac{1}{|\mathcal{S}|} \sum_{m \in \mathcal{S}} z_{m,i} \quad (3)$$

This normalization emphasizes directional agreement and captures the geometric structure of the item space independent of vector magnitude.

Leveraging these normalized consensus embeddings, we partition the item space into  $K$  disjoint clusters  $\{\mathcal{I}_k\}_{k=1}^K$  based on directional similarity. Specifically, we optimize the partition to maximize the within-cluster cosine similarity:

$$\{\mathcal{I}_k\}_{k=1}^K \leftarrow \arg \max_{\{\mathcal{I}_k\}} \sum_{k=1}^K \sum_{i \in \mathcal{I}_k} \cos(\tilde{e}_i, \mu_k) \quad (4)$$

where  $\mu_k$  denotes the centroid of the  $k$ -th cluster. We identify the anchor  $c_k$  as the item maximizing the cosine similarity to the centroid:

$$\mathcal{C} = \{c_k\}_{k=1}^K \quad \text{s.t. } c_k = \arg \max_{i \in \mathcal{I}_k} \cos(\tilde{e}_i, \mu_k) \quad (5)$$

The resulting coreset  $\mathcal{C}$  effectively preserves the global relational structure of the benchmark while acting as a robust basis for the subsequent extrapolation phase.

### 2.4. Extrapolation from Coreset to Full Benchmark

To evaluate an unseen target model  $t \in \mathcal{T}$ , we acquire its binary scores  $\{y_{t,i}\}_{i \in \mathcal{C}}$  on the selected coreset. We then employ a Ridge regression model  $g_t$  to extrapolate these local observations to the full benchmark.

Given the strictly limited coreset size, employing high-dimensional inputs induces high-variance fits. To ensure robustness, we construct a single scalar feature  $x_i$  for each item, defined as the average correctness across all source models:

$$x_i = \frac{1}{|\mathcal{S}|} \sum_{m \in \mathcal{S}} y_{m,i} \in [0, 1], \quad \forall i \in \mathcal{I} \quad (6)$$

This aggregated score serves as a robust input feature. We fit the regressor  $g_t$  by minimizing the squared error on the coreset:

$$g_t = \arg \min_g \frac{1}{|\mathcal{C}|} \sum_{i \in \mathcal{C}} (g(x_i) - y_{t,i})^2 \quad (7)$$

The optimized regressor yields predictions  $\hat{s}_{t,i} = g_t(x_i)$  for

all unobserved items, providing a robust linear approximation for the unseen items.

Finally, the global accuracy is derived by aggregating the ground-truth performance on  $\mathcal{C}$  with the predicted scores for the remaining items in  $\mathcal{I} \setminus \mathcal{C}$ . This formulation recovers both absolute performance and relative rankings while maintaining minimal computational overhead:

$$\widehat{\text{Acc}}(t) = \frac{1}{|\mathcal{I}|} \left( \sum_{i \in \mathcal{C}} y_{t,i} + \sum_{i \in \mathcal{I} \setminus \mathcal{C}} \hat{s}_{t,i} \right) \quad (8)$$

## 3. Main Experiments

### 3.1. Experimental Setup

**Benchmarks and Model Pools** We evaluate REP CORE on five benchmarks spanning text-only and multimodal domains. ARC Challenge (Clark et al., 2018) contains 1,172 science QA items evaluated by 96 models. BIG-Bench Hard (BBH) (Suzgun et al., 2023) includes 6,511 challenging reasoning items across 101 models. GSM8K (Cobbe et al., 2021) consists of 1,319 grade-school math word problems with 90 models. MMLU-Pro (Wang et al., 2024) contains 12,032 multi-domain questions evaluated by 91 models. SEED-Bench-2-Plus (Li et al., 2024) is a multimodal benchmark comprising 2,277 items and 93 models. A comprehensive list of models for each benchmark is provided in Appendix D.

**Implementation Details** We conduct all evaluations in the source-scarce regime, defined by  $|\mathcal{S}| = 10$ . For each benchmark, we randomly sample 10 models to form the source set  $\mathcal{S}$  and designate the remaining models as the target set  $\mathcal{T}$ . We report results averaged over 10 independent source/target splits. All model generations utilize greedy decoding to ensure reproducibility. To ensure fair comparison, all methods operate on identical splits and coreset sizes.

**Baselines and Metrics** We benchmark REP CORE against three output-based compression methods. *Random* selects the coreset via uniform random sampling. *AnchorPoints* (Vivek et al., 2024) represents items using their binary response vectors over  $\mathcal{S}$  and selects representative anchors via clustering in this discrete space. *GP-IRT* (Polo et al., 2024) employs a Gaussian Process-corrected Item Response Theory estimator to infer full-benchmark performance from the coreset evaluations.

We report two primary metrics on the target set  $\mathcal{T}$ : (i) *Spearman's rank correlation* ( $\rho$ ) between the predicted model rankings and the ground-truth rankings derived from full-benchmark accuracy; (ii) *Mean Absolute Error* (MAE) between the predicted and ground-truth accuracies.

Table 1. Main results. We report Spearman’s rank correlation ( $\rho, \uparrow$ ) and Mean Absolute Error (MAE,  $\downarrow$ ) on target models. The budget  $K$  denotes the number of items in the coresets. **Bold** and underlined values denote the best and second-best results, respectively.

Benchmark	Method	$K = 10$		$K = 20$		$K = 30$		$K = 40$		$K = 50$	
		$\rho \uparrow$	MAE $\downarrow$								
BBH	RANDOM	0.668	0.122	0.793	0.087	<u>0.852</u>	0.069	<u>0.884</u>	0.061	<u>0.905</u>	0.054
	ANCHORPOINTS	<u>0.701</u>	0.127	<u>0.799</u>	0.097	<u>0.835</u>	0.087	<u>0.854</u>	0.081	<u>0.867</u>	0.078
	GP-IRT	0.681	<b>0.093*</b>	0.786	<b>0.068*</b>	0.832	<u>0.058</u>	0.869	<u>0.052</u>	0.901	<b>0.045*</b>
	REPCORE	<b>0.718</b>	<u>0.095</u>	<b>0.824</b>	0.069	<b>0.870</b>	<b>0.057</b>	<b>0.898</b>	<b>0.049</b>	<b>0.913</b>	<b>0.045</b>
GSM8K	RANDOM	0.702	0.087	0.815	0.060	<u>0.870</u>	<u>0.049</u>	<u>0.898</u>	0.042	<u>0.917</u>	0.037
	ANCHORPOINTS	0.739	0.133	0.802	0.134	0.826	0.142	0.831	0.154	0.840	0.144
	GP-IRT	<u>0.750</u>	<b>0.069*</b>	0.839	<u>0.057</u>	0.857	0.051	0.865	<u>0.042</u>	0.896	<u>0.034</u>
	REPCORE	<b>0.763</b>	<u>0.071</u>	<b>0.872</b>	<b>0.047</b>	<b>0.905</b>	<b>0.039</b>	<b>0.926</b>	<b>0.035</b>	<b>0.938</b>	<b>0.032</b>
SEED-Bench-2-Plus	RANDOM	0.607	0.124	<u>0.728</u>	0.088	<u>0.800</u>	0.070	<u>0.836</u>	0.060	0.861	0.053
	ANCHORPOINTS	<b>0.653</b>	0.139	0.715	0.116	0.747	0.110	0.771	0.108	0.782	0.105
	GP-IRT	0.594	0.098	0.699	0.063	0.780	<b>0.050*</b>	0.824	<b>0.043*</b>	0.863	<b>0.038*</b>
	REPCORE	0.642	<b>0.084</b>	<b>0.755</b>	<b>0.060</b>	<b>0.819</b>	<u>0.051</u>	<b>0.853</b>	0.045	<b>0.874</b>	0.040

### 3.2. Main Results

We evaluate benchmark compression performance in the source-scarce regime with  $|\mathcal{S}| = 10$ . Table 1 summarizes the results on BBH, GSM8K, and SEED-Bench-2-Plus. Additional results for ARC Challenge and MMLU-Pro show consistent trends and are provided in Appendix C.2.

**REPCORE Effective Ranking and Reliable Extrapolation under Source Scarcity** As shown in Table 1, REPCORE consistently achieves stronger recovery of full-benchmark rankings. By leveraging consensus embeddings to recover the geometry of the item space, our method selects representative items even at small coresets sizes. For example, on GSM8K with  $K = 20$ , REPCORE attains a Spearman correlation of 0.872, surpassing GP-IRT at 0.839 and ANCHORPOINTS at 0.802. In terms of absolute performance estimation, REPCORE typically yields the lowest mean absolute error and improves steadily as  $K$  increases, maintaining a clear margin over baselines. Furthermore, extended analyses in Appendix C.9 indicate that REPCORE exhibits lower variance across experimental runs, demonstrating greater stability compared to baseline methods.

**Analysis of Prediction Fidelity** We observe that GP-IRT occasionally attains competitive MAE scores, marked with \*. However, this aggregate metric can mask item-level errors through cancellation. To assess prediction fidelity at the item level, we report the *Agreement* metric following Vivek et al. (2024), which measures the proportion of exact matches between predicted and ground-truth correctness labels. As detailed in Appendix C.1, GP-IRT exhibits substantially lower Agreement even when its MAE appears favorable. For instance, on BBH with  $K = 20$ , while GP-IRT matches REPCORE in MAE, its Agreement trails ours

by approximately 19 percentage points. This gap indicates that REPCORE better preserves the target model’s item-level correctness pattern.

## 4. Analysis of Aligned Representations

While the previous sections demonstrate the effectiveness of REPCORE in benchmark compression, a critical question remains regarding the interpretability of the learned representations: *Does the latent space merely act as a proxy for item difficulty, or does it capture richer, task-specific structural information?* To investigate this question, we analyze the geometric structure of the latent space in Section 4.2 and evaluate the utility of its principal components in Section 4.3.

### 4.1. Geometric Definition and Statistical Protocol

We conduct our primary analysis on benchmark **Big-Bench-Hard** to leverage its hierarchical taxonomy, which divides items into fine-grained subtasks and broader ability modes (see Appendix B.3 for detailed category definitions). This structure enables us to probe the granularity of the learned item representations.

**Analysis Protocol** We analyze the geometric properties of aligned embeddings across 100 model snapshots (10 combos  $\times$  10 models, align with the main experiment). The protocol proceeds in three steps:

**1. Embedding Projection and Decomposition** For each model snapshot  $m$  and item  $i$ , we first compute the aligned embedding  $z_{m,i} = f_\theta(\text{Proj}_m(h_{m,i})) \in \mathbb{R}^{32}$ . We aggregate these vectors for all items to form the embedding matrix  $Z_m \in \mathbb{R}^{|\mathcal{I}| \times 32}$ . Let  $\bar{z}_m$  denote the empirical mean of these embeddings. We then decompose the centered data via

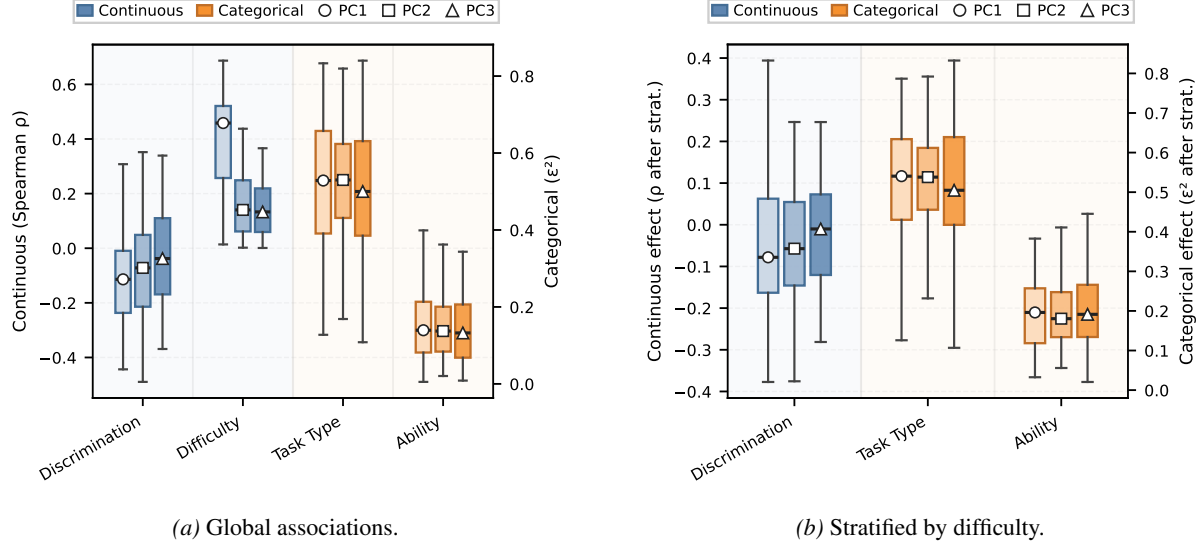


**Figure 3.** Factor-association analysis of the REPCORE latent space on BBH. Dual axes quantify associations: the left axis reports Spearman’s  $\rho$  for continuous factors (blue), while the right axis denotes effect size  $\epsilon^2$  for categorical factors (orange). Markers indicate principal components (Circle: PC<sub>1</sub>, Square: PC<sub>2</sub>, Triangle: PC<sub>3</sub>). (a) **Global Analysis:** The primary axis (PC<sub>1</sub>) is predominantly aligned with item difficulty ( $\rho \approx 0.46$ ), while categorical task identities also show strong initial associations. (b) **Stratified Analysis:** After controlling for difficulty through binning, the embeddings maintain a high clustering effect by fine-grained Task Type ( $\epsilon^2 \approx 0.54$ ), reinforcing the broader structural signal observed in coarse Ability Mode. This persistent structural signal confirms that the latent manifold encodes task-specific identities that transcend mere performance-based scalar signals.

PCA to derive the  $k$ -th principal axis  $w_m^{(k)}$ . Finally, the projection score  $\xi_{m,i}^{(k)}$  is computed by projecting the centered embedding onto this axis:  $\xi_{m,i}^{(k)} = \langle z_{m,i} - \bar{z}_m, w_m^{(k)} \rangle$ .

**2. Interpretable Factors** To investigate whether the learned representation recovers the intrinsic structural relationships among items in the benchmark, we evaluate the alignment between the projection scores  $\xi_{m,i}^{(k)}$  and four ground-truth attributes. Detailed computational formulations and definitions for these attributes are provided in the Appendix B.3 and B.4:

- **Continuous Factors:** Difficulty  $\delta_i$  (pass rate) and Discrimination  $\gamma_i$  (Kelley 27%  $D$ ).
- **Discrete Factors:** Subtask Identity  $\tau_i$  (fine-grained) and Ability Mode  $\alpha_i$  (coarse-grained).

**3. Statistical Association** To rigorously quantify the alignment between distinct principal components and the item attributes defined above, we propose a dual-granularity evaluation protocol centered on a unified association operator  $\mathcal{M}(\cdot)$ . This operator is realized as Spearman’s  $\rho$  for continuous attributes ( $\delta, \gamma$ ) and Kruskal-Wallis  $\epsilon^2$  for categorical ones ( $\tau, \alpha$ ), thereby providing a consistent measure to evaluate the representational geometry across two distinct granularities:

- **Global Analysis:** The macro-scale association is evaluated over the entire benchmark  $\mathcal{I}$  to capture general

trends:

$$\mathcal{A}_{\text{global}}^{(k,m)} = \mathcal{M} \left( \{\xi_{m,i}^{(k)}\}_{i \in \mathcal{I}}, \{\psi_i\}_{i \in \mathcal{I}} \right) \quad (9)$$

- **Stratified Analysis:** To isolate structural signals from the confounding effects of item difficulty, we partition  $\mathcal{I}$  into  $B = 20$  equi-sized bins  $\{\mathcal{I}_b\}_{b=1}^B$  based on  $\delta$ . Local statistics are then aggregated to derive a difficulty-invariant estimate:

$$\mathcal{A}_{\text{strat}}^{(k,m)} = \text{Agg} \left( \left\{ \mathcal{M} \left( \{\xi_{m,i}^{(k)}\}_{i \in \mathcal{I}_b}, \{\psi_i\}_{i \in \mathcal{I}_b} \right) \right\}_{b=1}^B \right) \quad (10)$$

where  $\text{Agg}(\cdot)$  denotes the aggregation of  $p$ -values via Stouffer’s method and effect sizes via Fisher- $z$  transformation, with full computational details deferred to the Appendix B.1.

To mitigate sampling variance, we aggregate these metrics over the full snapshot pool. Figure 3 summarizes the resulting empirical distributions via medians and interquartile ranges, offering a robust characterization of the representational geometry. Quantitatively, this characterization is statistically rigorous: both stratified  $p$ -values and FDR-corrected  $q$ -values consistently satisfy significance thresholds ( $\alpha = 0.05$ ) across snapshots, with medians often approaching floating-point limits (see Appendix B.2 for full results).

## 4.2. Disentangling Difficulty and Structure

**Global View: The Dominance of Difficulty** Globally (Figure 3a), PC<sub>1</sub> emerges as the dominant axis of variation, manifesting a strong correlation with item difficulty

$(\rho \approx 0.46)$ . While categorical factors such as subtask type exhibit substantial effect sizes ( $\epsilon^2 \approx 0.53$ ), we observe that this alignment is potentially susceptible to difficulty confounding. Specifically, if items within the same subtask share homogeneous complexity levels, global clustering may be a misleading artifact of difficulty rather than a reflection of task-specific reasoning patterns. This possibility necessitates a more granular investigation to adjudicate whether the captured signals are truly structural.

**Stratified View: Hierarchical Structural Persistence** To verify the persistence of structural identity, we move to a difficulty-stratified analysis (Figure 3b), which serves as a controlled setting to isolate task-specific signals from the aforementioned confounding effects. The results indicate that even within narrow difficulty bins, clustering by subtask type remains remarkably robust ( $\epsilon^2 \approx 0.54$ ). This resilience confirms that the aligned representations  $z_{m,i}$  encode fine-grained functional identities that transcend mere performance-based scalar signals. Moreover, this persistence further scales to the benchmark’s hierarchy, with the ability mode alignment ( $\epsilon^2 \approx 0.20$ ) confirming the recovery of abstract reasoning domains. These results suggest that the latent manifold preserves high-level cognitive modalities beyond granular task labels.

**The Role of Discrimination** In contrast to the dominant structural geometry, item discrimination acts as a secondary background signal, maintaining a modest yet stable negative correlation with  $PC_1$  across both global ( $\rho \approx -0.11$ ) and stratified ( $\rho \approx -0.08$ ) regimes. This suggests that while the bottleneck primarily optimizes for difficulty and structural features, it retains auxiliary information regarding the reliability of the item representations.

Table 2. Principal component ablation on BBH for performance extrapolation across  $K \in \{10, 20, 30, 40, 50\}$ .

$\rho \uparrow$	$K = 10$	$K = 20$	$K = 30$	$K = 40$	$K = 50$
$PC_1$	0.665	0.793	0.857	0.888	0.907
$PC_2$	0.662	0.794	0.853	0.887	0.907
$PC_3$	<u>0.689</u>	0.812	0.859	0.882	0.900
$PC_{1,2}$	<u>0.689</u>	0.812	<u>0.871</u>	<b>0.898</b>	<b>0.917</b>
$PC_{1,2,3}$	0.686	<u>0.820</u>	<b>0.875</b>	0.896	0.914
ALL	<b>0.718</b>	<b>0.824</b>	0.870	<b>0.898</b>	0.913
$MAE \downarrow$	$K = 10$	$K = 20$	$K = 30$	$K = 40$	$K = 50$
$PC_1$	<u>0.101</u>	0.074	0.060	0.053	0.048
$PC_2$	<u>0.101</u>	<u>0.070</u>	<u>0.058</u>	<u>0.050</u>	<b>0.045</b>
$PC_3$	0.103	0.072	0.060	0.052	0.047
$PC_{1,2}$	0.104	0.072	0.059	0.051	<b>0.045</b>
$PC_{1,2,3}$	0.104	0.073	<u>0.058</u>	0.051	<u>0.046</u>
ALL	<b>0.095</b>	<b>0.069</b>	<b>0.057</b>	<b>0.049</b>	<b>0.045</b>

### 4.3. Utility of the Interpretable Subspace

Building on the structural insights from the spectral analysis, we further evaluate how these interpretable dimensions

contribute to the core task of performance extrapolation. Table 2 presents the ablation results on the BBH benchmark, where we compare the predictive efficacy of individual principal components and low-rank subspaces against the full aligned representations across varying coresets budgets.

**Beyond Scalar Difficulty** While  $PC_1$  provides a robust predictive baseline by capturing item difficulty, the inclusion of  $PC_2$  and  $PC_3$  consistently enhances estimation fidelity. This improvement reinforces our geometric findings: higher-order components capture essential structural context including task identity and reasoning modalities. By leveraging these signals, the regressor can adjust for model-specific capabilities that a standard difficulty curve cannot account for.

**Robustness and Signal Concentration** A comparison with the full aligned embedding space reveals a distinct performance crossover. In extremely data-scarce regimes where  $K = 10$ , the full aligned embedding slightly outperforms the  $PC_{1,2}$  subspace. However, as the coresets size grows to  $K \geq 30$ , the  $PC_{1,2}$  subspace demonstrates superior robustness and eventually surpasses the full aligned embedding space. This shift suggests that while high-dimensional features may offer some utility at minimal sample sizes, they also introduce predictive instability. Conversely, the low-rank subspace concentrates the most generalizable signals to provide a stable basis for extrapolation without relying on the noise inherent in the high-dimensional manifold.

## 5. Ablations and Additional Analyses

**Continuous Representations Enable Superior Coreset Selection** To validate the necessity of our representation learning module, we conduct a controlled experiment by substituting the consensus embeddings with binary correctness vectors during the clustering phase, while maintaining the identical downstream extrapolation mechanism. Table 4 reports the average performance with  $K = 30$ . The results indicate that relying on discrete correctness signals yields inferior ranking correlation and higher estimation error. This performance gap confirms that the continuous embedding space preserves fine-grained item distinctions essential for representative sampling, which are not captured by binary correctness signals. Detailed per-dataset results are provided in Appendix C.3.

**Aligned Representations Are Data-Efficient in Source-Scarce Regimes** We evaluate the data efficiency of our framework by varying the source pool size  $|\mathcal{S}|$ . Table 3 presents the performance metrics as the number of source models increases from 5 to 20 with  $K = 30$ . REP-CORE demonstrates strong stability even in highly resource-constrained scenarios. Under the most restricted setting with

Table 3. Performance averaged over five benchmarks for varying source pool sizes with  $K = 30$ .

Method	$ \mathcal{S}  = 5$		$ \mathcal{S}  = 10$		$ \mathcal{S}  = 15$		$ \mathcal{S}  = 20$	
	$\rho \uparrow$	MAE $\downarrow$	$\rho \uparrow$	MAE $\downarrow$	$\rho \uparrow$	MAE $\downarrow$	$\rho \uparrow$	MAE $\downarrow$
ANCHORPOINTS	0.640	0.210	0.809	0.116	0.848	0.091	0.861	0.080
GP-IRT	0.822	0.057	0.836	0.053	0.843	<b>0.049</b>	0.828	0.050
<b>REPCORE</b>	<b>0.860</b>	<b>0.052</b>	<b>0.868</b>	<b>0.049</b>	<b>0.860</b>	<b>0.049</b>	<b>0.864</b>	<b>0.049</b>

Table 4. Ablation on clustering inputs averaged over five benchmarks with  $K = 30$ .

Clustering Input	$\rho \uparrow$	MAE $\downarrow$
Correctness Vectors	0.850	0.055
<b>Consensus Embeddings</b>	<b>0.868</b>	<b>0.049</b>

only five source models, output-based methods, including ANCHORPOINTS, exhibit a substantial performance drop. In contrast, REPCORE achieves a Spearman correlation of 0.860, which significantly outperforms baselines. Furthermore, the performance of our framework stabilizes rapidly as the source pool expands. This saturation indicates that the aligned space effectively recovers the geometry of the item space under minimal supervision, thereby reducing the dependency on extensive source model pools. Detailed per-dataset results are provided in Appendix C.4

**Impact of Source Model Composition** We investigate how source pool diversity affects compression quality. Table 5 indicates that a diverse composition of model families and capability ranges yields the most robust performance. Relying on a single model family introduces architectural biases, as evidenced by the performance drop in single-family pools. Similarly, homogeneous pools restricted to a narrow capability range prove suboptimal, as they fail to simultaneously maintain high ranking correlation and low estimation error. These findings suggest that incorporating diverse sources mitigates architectural and capability biases, allowing the aligned representations to better capture the geometry of the item space that supports reliable extrapolation. Detailed per-dataset results are provided in Appendix C.5 and Appendix C.6.

Table 5. Performance comparison under varied source compositions averaged across five benchmarks at  $K = 30$ .

Composition	Setting	$\rho \uparrow$	MAE $\downarrow$
Model Family	Family A <sup>†</sup>	0.848	0.057
	Family B <sup>‡</sup>	0.686	0.058
	Diverse (Ours)	<b>0.868</b>	<b>0.049</b>
Capability	Strong Only	0.778	0.092
	Weak Only	0.799	0.055
	Diverse (Ours)	<b>0.868</b>	<b>0.049</b>

<sup>†</sup> Qwen / Ovis; <sup>‡</sup> Llama / InternVLLM.

**Scalability to Larger Coreset Budgets** We further examine scalability by increasing the coreset budget to  $K = 100$ , 150, and 200. As shown in Table 6, REPCORE improves steadily as  $K$  increases and maintains strong ranking and estimation accuracy relative to baselines. These results indicate that the learned item space continues to support effective coreset selection at larger budgets. Detailed per-dataset results are provided in Appendix C.7.

Table 6. Average performance across benchmarks with larger coreset budgets.

Method	$K = 100$		$K = 150$		$K = 200$	
	$\rho \uparrow$	MAE $\downarrow$	$\rho \uparrow$	MAE $\downarrow$	$\rho \uparrow$	MAE $\downarrow$
RANDOM	0.947	0.033	0.964	0.027	0.972	0.023
ANCHOR POINTS	0.833	0.111	0.832	0.107	0.836	0.099
GP-IRT	<b>0.951</b>	<b>0.027</b>	<b>0.966</b>	<b>0.023</b>	<b>0.973</b>	<b>0.021</b>
<b>REPCORE</b>	<b>0.954</b>	0.028	<b>0.967</b>	<b>0.023</b>	<b>0.975</b>	<b>0.021</b>

**Robustness to Temporal Distribution Shift** Rapid progress in LLMs induces temporal shifts in model behaviors. We simulate such shifts by constructing the source pool from the oldest 30% of models and extrapolating performance for the remaining held-out models under this chronological split. As shown in Table 7, REPCORE achieves the strongest ranking performance while maintaining competitive estimation error. This result is consistent with our premise that the learned item space captures stable item-level structure and remains effective as the model pool evolves. Detailed per-dataset results are provided in Appendix C.8.

Table 7. Temporal generalization under a chronological split with historical sources and  $K = 30$ .

Method	$\rho \uparrow$	MAE $\downarrow$
RANDOM	0.845	0.060
ANCHORPOINTS	0.797	0.110
GP-IRT	0.835	<b>0.049</b>
<b>REPCORE</b>	<b>0.853</b>	0.050

## 6. Conclusion and Future Work

In this work, we introduce REPCORE, a framework leveraging aligned representations to identify representative benchmark subsets. Our evaluation confirms that REPCORE sig-

nificantly outperforms output-based baselines in ranking correlation and estimation accuracy, while maintaining robust performance under source model scarcity and temporal distribution shifts. For future directions, we aim to extend this paradigm to closed-source models, thereby establishing a unified standard for open and proprietary systems. Furthermore, exploring the cross-domain transferability of aligned representations promises to enable efficient coresnet selection for specialized domains without task-specific retraining.

## Impact Statement

This paper presents work whose goal is to advance the field of Machine Learning. There are many potential societal consequences of our work, none which we feel must be specifically highlighted here.

## References

Achiam, J., Adler, S., Agarwal, S., Ahmad, L., Akkaya, I., Aleman, F. L., Almeida, D., Altenschmidt, J., Altman, S., Anadkat, S., et al. Gpt-4 technical report. [arXiv preprint arXiv:2303.08774](#), 2023.

Azaria, A. and Mitchell, T. The internal state of an llm knows when it's lying. [arXiv preprint arXiv:2304.13734](#), 2023.

Clark, P., Cowhey, I., Etzioni, O., Khot, T., Sabharwal, A., Schoenick, C., and Tafjord, O. Think you have solved question answering? try arc, the ai2 reasoning challenge. [arXiv preprint arXiv:1803.05457](#), 2018.

Cobbe, K., Kosaraju, V., Bavarian, M., Chen, M., Jun, H., Kaiser, L., Plappert, M., Tworek, J., Hilton, J., Nakano, R., et al. Training verifiers to solve math word problems. [arXiv preprint arXiv:2110.14168](#), 2021.

Dubey, A., Jauhri, A., Pandey, A., Kadian, A., Al-Dahle, A., Letman, A., Mathur, A., Schelten, A., Yang, A., Fan, A., et al. The llama 3 herd of models. [arXiv e-prints](#), pp. arXiv–2407, 2024.

Gupta, V., Ross, C., Pantoja, D., Passonneau, R. J., Ung, M., and Williams, A. Improving model evaluation using smart filtering of benchmark datasets. In [Proceedings of the 2025 Conference of the Nations of the Americas Chapter of the Association for Computational Linguistics: Human Language Technologies \(Volume 1: Long Papers\)](#), pp. 4595–4615, 2025.

Li, B., Ge, Y., Chen, Y., Ge, Y., Zhang, R., and Shan, Y. Seed-bench-2-plus: Benchmarking multimodal large language models with text-rich visual comprehension. [arXiv preprint arXiv:2404.16790](#), 2024.

Li, K., Patel, O., Viégas, F., Pfister, H., and Wattenberg, M. Inference-time intervention: Eliciting truthful answers from a language model. [Advances in Neural Information Processing Systems](#), 36:41451–41530, 2023.

Liang, P., Bommasani, R., Lee, T., Tsipras, D., Soylu, D., Yasunaga, M., Zhang, Y., Narayanan, D., Wu, Y., Kumar, A., et al. Holistic evaluation of language models. [arXiv preprint arXiv:2211.09110](#), 2022.

Lugoloobi, W. and Russell, C. Llms encode how difficult problems are. [arXiv preprint arXiv:2510.18147](#), 2025.

Ma, Z., Yuan, Q., Wang, Z., and Zhou, D. Large language models have intrinsic meta-cognition, but need a good lens. [arXiv preprint arXiv:2506.08410](#), 2025.

Marjanović, S. V., Patel, A., Adlakha, V., Aghajohari, M., BehnamGhader, P., Bhatia, M., Khandelwal, A., Kraft, A., Krojer, B., Lù, X. H., et al. Deepseek-r1 thoughtology: Let's think about llm reasoning. [arXiv preprint arXiv:2504.07128](#), 2025.

Orgad, H., Toker, M., Gekhman, Z., Reichart, R., Szpektor, I., Kotek, H., and Belinkov, Y. Llms know more than they show: On the intrinsic representation of llm hallucinations. [arXiv preprint arXiv:2410.02707](#), 2024.

Perlitz, Y., Bandel, E., Gera, A., Ariviv, O., Dor, L. E., Shnarch, E., Slonim, N., Shmueli-Scheuer, M., and Choshen, L. Efficient benchmarking (of language models). In [Proceedings of the 2024 Conference of the North American Chapter of the Association for Computational Linguistics: Human Language Technologies \(Volume 1: Long Papers\)](#), pp. 2519–2536, 2024.

Polo, F. M., Weber, L., Choshen, L., Sun, Y., Xu, G., and Yurochkin, M. tinybenchmarks: evaluating llms with fewer examples. [arXiv preprint arXiv:2402.14992](#), 2024.

Suzgun, M., Scales, N., Schärli, N., Gehrman, S., Tay, Y., Chung, H. W., Chowdhery, A., Le, Q., Chi, E., Zhou, D., et al. Challenging big-bench tasks and whether chain-of-thought can solve them. In [Findings of the Association for Computational Linguistics: ACL 2023](#), pp. 13003–13051, 2023.

Vivek, R., Ethayarajh, K., Yang, D., and Kiela, D. Anchor points: Benchmarking models with much fewer examples. In [Proceedings of the 18th Conference of the European Chapter of the Association for Computational Linguistics \(Volume 1: Long Papers\)](#), pp. 1576–1601, 2024.

Wang, Y., Ma, X., Zhang, G., Ni, Y., Chandra, A., Guo, S., Ren, W., Arulraj, A., He, X., Jiang, Z., et al. Mmlu-pro: A more robust and challenging multi-task language understanding benchmark. [Advances in Neural Information Processing Systems](#), 37:95266–95290, 2024.

Wang, Y., Li, H., Zou, H., Zhang, J., He, X., Li, Q., and Xu, K. Faclens: Transferable probe for foreseeing non-factuality in fact-seeking question answering of large language models. In Proceedings of the 2025 Conference on Empirical Methods in Natural Language Processing, pp. 18574–18593, 2025a.

Wang, Y., Ying, J., Cao, Y., Ma, Y., and Jiang, Y. Effieval: Efficient and generalizable model evaluation via capability coverage maximization. arXiv preprint arXiv:2508.09662, 2025b.

Yang, A., Li, A., Yang, B., Zhang, B., Hui, B., Zheng, B., Yu, B., Gao, C., Huang, C., Lv, C., et al. Qwen3 technical report. arXiv preprint arXiv:2505.09388, 2025.

Yuan, P., Zhang, Y., Feng, S., Li, Y., Wang, X., Shi, J., Tan, C., Pan, B., Hu, Y., and Li, K. Beyond one-size-fits-all: Tailored benchmarks for efficient evaluation. arXiv preprint arXiv:2502.13576, 2025.

Zhang, A., Chen, Y., Pan, J., Zhao, C., Panda, A., Li, J., and He, H. Reasoning models know when they’re right: Probing hidden states for self-verification. arXiv preprint arXiv:2504.05419, 2025.

Zhu, Y., Liu, D., Lin, Z., Tong, W., Zhong, S., and Shao, J. The llm already knows: Estimating llm-perceived question difficulty via hidden representations. In Proceedings of the 2025 Conference on Empirical Methods in Natural Language Processing, pp. 1160–1176, 2025.

Zou, A., Phan, L., Chen, S., Campbell, J., Guo, P., Ren, R., Pan, A., Yin, X., Mazeika, M., Dombrowski, A.-K., et al. Representation engineering: A top-down approach to ai transparency. arXiv preprint arXiv:2310.01405, 2023.

## A. Related Work

### A.1. Benchmark Compression

*benchmark compression* aims to select a minimal subset of items that preserves full-benchmark rankings and enables accurate score estimation. Existing methods can be categorized based on the signals they utilize: prediction outputs versus input/internal features.

**Prediction-Based Coreset Selection.** The dominant paradigm relies on the correlation of model outputs (i.e., accuracy) across test items. ANCHOR POINTS (Vivek et al., 2024) and TAILED BENCHMARKS (Yuan et al., 2025) represent each item by its “prediction pattern”—a vector of correctness scores derived from a population of source models. By applying clustering to these patterns, they identify items that maximize information gain. Similarly, TINYBENCHMARKS (Polo et al., 2024) adopts Item Response Theory (IRT) to fit latent discrimination and difficulty parameters from response patterns. A critical limitation of these methods is the “cold start” problem: they require a diverse pool of source models to construct robust prediction pattern. In low-resource regimes (e.g., few source models), the sparse binary signal (correct/incorrect) is often insufficient to capture fine-grained dataset structures.

**Feature-Based and Heuristic Filtering.** Alternative approaches utilize static semantic features or internal model statistics. SMART (Gupta et al., 2025) filters datasets by removing samples that are semantically redundant (measured via textual embedding distance) or statistically “easy” for models. More recently, EFFIEVAL (Wang et al., 2025b) proposes a training-free selection method that maximizes the coverage of activated neurons, positing that diverse activation patterns correspond to diverse model capabilities. While EFFIEVAL leverages internal signals, it focuses on neuron-level coverage for sampling rather than aligning latent spaces for structural recovery. Our work advances this direction by exploiting the continuous hidden states to characterize item structure, providing a denser signal than discrete outputs while avoiding the need for massive source model populations.

### A.2. Internal Representations and Difficulty Perception

Beyond their use in compression, hidden states have been extensively studied for their ability to encode task-level properties.

**Probing for Factuality.** Representation engineering has shown that LLM hidden states contain linearly separable directions corresponding to truthfulness. Methods like SAPLMA (Azaria & Mitchell, 2023) and FACLENS (Wang et al., 2025a) train probes to detect hallucinations or predict correctness before generation is complete, suggesting models possess intrinsic meta-cognition regarding their knowledge boundaries (Ma et al., 2025; Orgad et al., 2024).

**Encoding Difficulty and Structure.** Recent findings indicate that hidden representations also implicitly encode the complexity of input queries. Zhu et al. (2025) and Lugoloobi & Russell (2025) demonstrate that the difficulty of a question can be estimated directly from its hidden states or attention patterns, often aligning better with model performance than human-labeled difficulty. Unlike prior works that use these signals primarily for difficulty estimation or inference-time intervention (Li et al., 2023), we propose REP CORE to leverage these high-dimensional, density-rich signals for benchmark compression. By treating hidden states as a continuous proxy for item characteristics, we can recover dataset structures more effectively than methods relying on sparse discrete labels.

## B. Methodological Details

### B.1. Aggregation Operator for Stratified Associations

This section formalizes the aggregation operator  $\text{Agg}(\cdot)$  used in the stratified analysis protocol (Section 2.1). Let  $\{\mathcal{I}_b\}_{b=1}^B$  denote the difficulty-stratified partition of the benchmark item set  $\mathcal{I}$ . For each bin  $\mathcal{I}_b$ , the within-bin procedure  $\mathcal{M}(\cdot)$  produces a pair  $(\eta_b, p_b)$ , where  $\eta_b$  is an effect-size statistic and  $p_b$  is the corresponding  $p$ -value (bins with undefined outputs are excluded from aggregation). Let  $n_b$  be the number of valid items contributing to  $\mathcal{M}(\cdot)$  in bin  $b$ . To account for varying bin sample sizes in the aggregation, we assign each bin the weight  $w_b = \sqrt{n_b}$ .

**Aggregation of  $p$ -values (weighted Stouffer)** Let  $p_b$  denote the  $p$ -value computed on bin  $b$ . We convert  $p_b$  to a normal score  $s_b$  by

$$s_b = \begin{cases} \Phi^{-1}(1 - p_b), & \text{Kruskal–Wallis (one-sided),} \\ \Phi^{-1}\left(1 - \frac{p_b}{2}\right), & \text{Spearman (two-sided).} \end{cases} \quad (11)$$

The weighted Stouffer statistic is

$$Z_{\text{st}} = \frac{\sum_b w_b s_b}{\sqrt{\sum_b w_b^2}}. \quad (12)$$

Accordingly, the stratified  $p$ -value is

$$p_{\text{strat}} = \begin{cases} 1 - \Phi(Z_{\text{st}}), & \text{Kruskal–Wallis,} \\ 2(1 - \Phi(|Z_{\text{st}}|)), & \text{Spearman,} \end{cases} \quad (13)$$

where  $\Phi(\cdot)$  denotes the standard normal CDF.

**Aggregation of effect sizes** Effect sizes are aggregated separately for continuous and discrete attributes.

- **Continuous attributes (Spearman).** Let  $\rho_b$  denote the Spearman correlation computed on bin  $b$ . Correlations are combined via the Fisher transformation with inverse-variance weights:

$$\zeta = \frac{\sum_b (n_b - 3) \operatorname{arctanh}(\rho_b)}{\sum_b (n_b - 3)}, \quad (14)$$

$$\rho_c = \tanh(\zeta), \quad (15)$$

where  $(n_b - 3)$  is the standard inverse-variance weight under Fisher’s transformation. The aggregated correlation  $\rho_c$  is reported as the stratified effect size.

- **Discrete attributes (Kruskal–Wallis).** Let  $H_b$  denote the Kruskal–Wallis statistic computed on bin  $b$ , using  $n_b$  valid items across  $g_b$  retained groups. The within-bin effect size is quantified by epsilon-squared:

$$\epsilon_b^2 = \max\left\{0, \frac{H_b - g_b + 1}{n_b - g_b}\right\}. \quad (16)$$

The stratified effect size is the mean of within-bin estimates, weighted by their respective sample sizes  $n_b$ :

$$\epsilon_{\text{strat}}^2 = \frac{\sum_b n_b \epsilon_b^2}{\sum_b n_b}. \quad (17)$$

**Multiple testing control** Let  $\Psi$  denote the set of tested item attributes. For each fixed principal component index  $k$ , we apply Benjamini–Hochberg FDR correction to the collection of stratified  $p$ -values  $\{p_{\text{strat}}(\psi)\}_{\psi \in \Psi}$ . The resulting per-component adjusted values are reported as  $q_{\text{strat,pcwise}}$ .

## B.2. Detailed Statistical Distributions of Aligned Representations

To complement the summary statistics provided in the main text, we report the detailed distribution of statistical association metrics across the 100 model snapshots. Table 8 presents the median, 25th percentile, and 75th percentile for both the global  $p$ -values (derived from Spearman’s  $\rho$ ) and the stratified FDR-corrected  $q$ -values ( $q_{\text{strat}}$ ).

As observed, the associations are overwhelmingly significant. For the difficulty-stratified analysis, the median  $q_{\text{strat}}$  values for the first three principal components (PC<sub>1</sub>–PC<sub>3</sub>) are consistently below  $10^{-190}$ , approaching the numerical precision limits of standard floating-point representations. These results confirm that the geometric alignment captured by REP CORE is statistically robust and not an artifact of specific source model sampling.

## B.3. BBH Taxonomy and Ability Mapping

Table 9 summarizes the BBH subtask grouping used in our analysis. Since BBH contains heterogeneous subtasks with different reasoning demands, we consolidate the fine-grained task names into five broader ability modes (Logical, Language, Mathematical, Spatial/Temporal, and Knowledge/Domain). This mapping provides a consistent level of abstraction for reporting and interpreting stratified results at the ability level, while retaining the original BBH taxonomy at the subtask level.

**Table 8. Distribution of Statistical Significance Metrics.** We report the empirical distribution (Median, 25<sup>th</sup>, and 75<sup>th</sup> percentiles) of significance tests across 100 model snapshots. “Global” metrics correspond to raw Spearman correlations, while “Stratified” metrics denote the FDR-corrected  $q$ -values ( $q_{\text{strat}}$ ) after controlling for difficulty. Note that values displayed as 0 indicate probabilities below the numerical precision limit (underflow).

Mode	Component	Metric	Median	25% Percentile	75% Percentile	IQR
GLOBAL	PC1	$p$	$4.16 \times 10^{-249}$	0	$6.96 \times 10^{-70}$	$6.96 \times 10^{-70}$
	PC2	$p$	$2.07 \times 10^{-129}$	0	$2.02 \times 10^{-30}$	$2.02 \times 10^{-30}$
	PC3	$p$	$7.46 \times 10^{-109}$	0	$3.96 \times 10^{-26}$	$3.96 \times 10^{-26}$
STRATIFIED	PC1	$p$	$1.27 \times 10^{-204}$	0	$3.41 \times 10^{-65}$	$3.41 \times 10^{-65}$
		$q_{\text{strat}}$	$3.18 \times 10^{-204}$	0	$5.69 \times 10^{-65}$	$5.69 \times 10^{-65}$
	PC2	$p$	$1.76 \times 10^{-193}$	0	$4.56 \times 10^{-60}$	$4.56 \times 10^{-60}$
		$q_{\text{strat}}$	$4.39 \times 10^{-193}$	0	$5.88 \times 10^{-60}$	$5.88 \times 10^{-60}$
	PC3	$p$	$5.25 \times 10^{-203}$	0	$1.57 \times 10^{-59}$	$1.57 \times 10^{-59}$
		$q_{\text{strat}}$	$1.31 \times 10^{-202}$	0	$1.96 \times 10^{-59}$	$1.96 \times 10^{-59}$

**Table 9. BBH taxonomy and task grouping.**

Ability	Subtasks
<b>Logical</b>	boolean_expressions, dyck_languages, formal_fallacies, web_of_lies, logical_deduction_{three, five, seven}_objects
<b>Language</b>	disambiguation_qa, hyperbaton, ruin_names, salient_translation_error_detection, snarks
<b>Mathematical</b>	geometric_shapes, multistep_arithmetic_two, object_counting, word_sorting
<b>Spatial/Temporal</b>	date_understanding, navigate, temporal_sequences, tracking_shuffled_objects_{three, five, seven}_objects
<b>Knowledge/Domain</b>	causal_judgement, movie_recommendation, penguins_in_a_table, reasoning_about_colored_objects, sports_understanding

#### B.4. Computation of Continuous Factors

All continuous item factors are computed from responses of the full evaluated model set  $\mathcal{U} = \mathcal{S} \cup \mathcal{T}$ . Let  $a_{m,i} \in \{0, 1\}$  indicate whether model  $m \in \mathcal{U}$  answers item  $i$  correctly.

**Difficulty** ( $\delta_i$ ). Item difficulty is defined as the pass rate across the full evaluated models:

$$\delta_i = \frac{1}{|\mathcal{U}|} \sum_{m \in \mathcal{U}} a_{m,i}. \quad (18)$$

Lower values of  $\delta_i$  correspond to more difficult items.

**Discrimination** ( $\gamma_i$ ; Kelley 27%  $D$ ) Item discrimination is defined using Kelley’s 27% high–low criterion. Each model is first assigned an overall benchmark score

$$r_m = \frac{1}{|\mathcal{I}|} \sum_{j \in \mathcal{I}} a_{m,j}, \quad (19)$$

where  $\mathcal{I}$  denotes the item set of the benchmark. Let  $q = \max\{1, \lfloor 0.27|\mathcal{U}|\rfloor\}$ , and let  $\mathcal{U}_{\text{hi}}$  and  $\mathcal{U}_{\text{lo}}$  denote the top- $q$  and bottom- $q$  models under  $r_m$ , respectively. For each item  $i$ , the high/low-group pass rates and the Kelley discrimination score

are defined as

$$\begin{aligned}\pi_i^{\text{hi}} &= \frac{1}{|\mathcal{U}_{\text{hi}}|} \sum_{m \in \mathcal{U}_{\text{hi}}} a_{m,i}, \\ \pi_i^{\text{lo}} &= \frac{1}{|\mathcal{U}_{\text{lo}}|} \sum_{m \in \mathcal{U}_{\text{lo}}} a_{m,i}, \\ \gamma_i &= D_i = \pi_i^{\text{hi}} - \pi_i^{\text{lo}}.\end{aligned}\tag{20}$$

A higher  $\gamma_i$  signifies a more pronounced separation between models with high and low performance.

## C. More Experimental Results

### C.1. Detailed Item-level Agreement Results

Motivated by an observation in the main results that GP-IRT can achieve deceptively low MAE, Table 10 reports an **item-level Agreement** metric across budgets  $K \in \{10, 20, 30, 40, 50\}$ , measuring the fraction of items whose predicted correctness labels exactly match the ground truth. Agreement reveals that a low MAE does not necessarily imply faithful extrapolation: MAE can be artificially reduced when a method shrinks predictions toward the global mean or benefits from error cancellation.

Across all benchmarks and budgets, REP CORE consistently achieves the best Agreement, indicating that our predictions preserve the fine-grained per-item error pattern rather than merely matching averages. Therefore, we treat Agreement as a complementary fidelity check and caution against using MAE alone as the primary indicator of extrapolation quality.

*Table 10. Item-level Agreement across budgets.* Agreement ( $\uparrow$ ) over  $K \in \{10, 20, 30, 40, 50\}$ ; RANDOM is excluded as it does not extrapolate beyond the coreset. **Bold** and underline denote the best and second-best results.

Benchmark	Method	$K = 10$	$K = 20$	$K = 30$	$K = 40$	$K = 50$
ARC-Challenge	ANCHORPOINTS	0.760	0.741	0.736	0.730	0.731
	GP-IRT	<u>0.811</u>	<u>0.806</u>	<u>0.806</u>	<u>0.822</u>	<u>0.838</u>
	REP CORE	<b>0.848</b>	<b>0.858</b>	<b>0.862</b>	<b>0.865</b>	<b>0.867</b>
BBH	ANCHORPOINTS	0.612	0.626	0.630	0.634	0.634
	GP-IRT	<u>0.618</u>	<u>0.631</u>	<u>0.645</u>	<u>0.672</u>	<u>0.693</u>
	REP CORE	<b>0.697</b>	<b>0.714</b>	<b>0.721</b>	<b>0.725</b>	<b>0.727</b>
GSM8K	ANCHORPOINTS	0.767	0.756	0.747	0.733	0.745
	GP-IRT	<u>0.820</u>	<u>0.824</u>	<u>0.835</u>	<u>0.851</u>	<u>0.863</u>
	REP CORE	<b>0.863</b>	<b>0.876</b>	<b>0.881</b>	<b>0.884</b>	<b>0.886</b>
MMLU_Pro	ANCHORPOINTS	0.603	0.627	0.629	0.629	0.631
	GP-IRT	<u>0.611</u>	<u>0.651</u>	<u>0.685</u>	<u>0.713</u>	<u>0.730</u>
	REP CORE	<b>0.726</b>	<b>0.744</b>	<b>0.751</b>	<b>0.754</b>	<b>0.756</b>
SEED-Bench-2-Plus	ANCHORPOINTS	0.654	0.667	0.670	0.669	0.671
	GP-IRT	0.594	0.618	<u>0.670</u>	<u>0.718</u>	<u>0.749</u>
	REP CORE	<b>0.769</b>	<b>0.784</b>	<b>0.791</b>	<b>0.794</b>	<b>0.797</b>

### C.2. Additional Main Results on ARC-Challenge and MMLU-Pro

Table 11 extends the main-budget evaluation to ARC-Challenge and MMLU-Pro under the same source-scARCe protocol, reporting Spearman's  $\rho$  and MAE across budgets  $K \in \{10, 20, 30, 40, 50\}$ . The overall trend matches the main text: REP CORE improves monotonically with  $K$  and achieves the strongest ranking recovery once the budget leaves the extremely small regime, delivering the best  $\rho$  on both benchmarks for  $K \geq 20$ .

In terms of MAE, REP CORE remains competitive across budgets and often excels at small-to-moderate  $K$ , while GP-IRT can appear slightly better on MMLU-Pro at larger  $K$ . However, as discussed in Appendix C.1, MAE can be reduced by averaging effects and error cancellation. Together with Table 10, these results suggest that REP CORE achieves reliable ranking recovery while better preserving per-item correctness.

Table 11. Additional main results. We report Spearman’s rank correlation ( $\rho$ ,  $\uparrow$ ) and Mean Absolute Error (MAE,  $\downarrow$ ). **Bold** and underline indicate the best and second-best results among competitive methods, respectively.

Benchmark	Method	$K = 10$		$K = 20$		$K = 30$		$K = 40$		$K = 50$	
		$\rho \uparrow$	MAE $\downarrow$								
ARC-Challenge	RANDOM	0.681	0.089	0.801	0.061	<u>0.856</u>	<u>0.051</u>	0.888	0.043	0.908	0.038
	ANCHORPOINTS	<b>0.724</b>	0.132	0.767	0.136	0.792	0.138	0.797	0.145	0.796	0.143
	GP-IRT	0.706	<u>0.076</u>	<u>0.808</u>	<u>0.057</u>	0.845	0.052	0.866	<u>0.043</u>	0.884	<u>0.036</u>
	REPCORE	<u>0.707</u>	<b>0.072</b>	<b>0.820</b>	<b>0.050</b>	<b>0.871</b>	<b>0.041</b>	<b>0.900</b>	<b>0.036</b>	<b>0.921</b>	<b>0.032</b>
MMLU_Pro	RANDOM	0.702	0.124	0.812	0.088	0.865	0.071	0.895	0.062	0.914	0.055
	ANCHORPOINTS	<b>0.754</b>	0.140	0.800	0.107	0.846	0.102	0.861	0.095	0.867	0.095
	GP-IRT	0.646	<u>0.101</u>	<u>0.806</u>	<b>0.065*</b>	<u>0.866</u>	<b>0.053*</b>	<u>0.899</u>	<b>0.046*</b>	<u>0.920</u>	<b>0.041*</b>
	REPCORE	<u>0.732</u>	<b>0.091</b>	<b>0.829</b>	<u>0.067</u>	<b>0.875</b>	<u>0.055</u>	<b>0.906</b>	<u>0.048</u>	<b>0.924</b>	0.043

Table 12. Discrete-representation ablation. Per-dataset results comparing REPCORE with a discrete clustering variant (0/1 K-MEANS+RIDGE). We report Spearman’s  $\rho$  ( $\uparrow$ ) and MAE ( $\downarrow$ ) across budgets  $K \in \{10, 20, 30, 40, 50\}$ . **Bold** indicates the best result.

Benchmark	Method	$K = 10$		$K = 20$		$K = 30$		$K = 40$		$K = 50$	
		$\rho \uparrow$	MAE $\downarrow$								
ARC-Challenge	0/1 K-MEANS+RIDGE	0.685	<b>0.0719</b>	0.803	0.0578	0.850	0.0512	0.874	0.0485	0.894	0.0449
	REPCORE	<b>0.707</b>	0.0720	<b>0.820</b>	<b>0.0500</b>	<b>0.871</b>	<b>0.0409</b>	<b>0.900</b>	<b>0.0358</b>	<b>0.921</b>	<b>0.0321</b>
BBH	0/1 K-MEANS+RIDGE	0.717	0.0958	0.821	0.0713	0.862	0.0604	0.884	0.0533	0.896	0.0487
	REPCORE	<b>0.718</b>	<b>0.0950</b>	<b>0.824</b>	<b>0.0687</b>	<b>0.870</b>	<b>0.0569</b>	<b>0.898</b>	<b>0.0494</b>	<b>0.913</b>	<b>0.0452</b>
GSM8K	0/1 K-MEANS+RIDGE	0.754	0.0745	0.845	0.0579	0.886	0.0514	0.909	0.0471	0.922	0.0442
	REPCORE	<b>0.763</b>	<b>0.0714</b>	<b>0.872</b>	<b>0.0473</b>	<b>0.905</b>	<b>0.0393</b>	<b>0.926</b>	<b>0.0350</b>	<b>0.938</b>	<b>0.0316</b>
SEED-Bench-2-Plus	0/1 K-MEANS+RIDGE	0.514	0.0860	0.697	0.0656	0.786	0.0566	0.829	0.0511	0.857	0.0473
	REPCORE	<b>0.642</b>	<b>0.0835</b>	<b>0.755</b>	<b>0.0600</b>	<b>0.819</b>	<b>0.0508</b>	<b>0.853</b>	<b>0.0446</b>	<b>0.874</b>	<b>0.0402</b>
MMLU-Pro	0/1 K-MEANS+RIDGE	0.725	<b>0.0874</b>	0.824	0.0685	0.865	0.0575	0.890	0.0505	0.904	0.0462
	REPCORE	<b>0.732</b>	0.0910	<b>0.829</b>	<b>0.0666</b>	<b>0.875</b>	<b>0.0548</b>	<b>0.906</b>	<b>0.0476</b>	<b>0.924</b>	<b>0.0426</b>

### C.3. Discrete-Representation Ablation

Table 12 presents a controlled ablation that isolates the contribution of continuous aligned representations in the coresets selection stage. We replace our consensus embeddings with concatenated binary correctness vectors and perform clustering in this discrete space (0/1 K-MEANS+RIDGE), while keeping the downstream extrapolation module identical. This design ensures that any performance difference is attributable to the representation used for summarizing item structure rather than the predictor itself.

Across all datasets, REPCORE consistently yields higher (or comparable) Spearman correlation and lower MAE for most budgets, with the largest gains appearing on benchmarks where item structure is richer (e.g., multimodal SEED-Bench-2-Plus). While the discrete baseline can be competitive on MAE at the smallest budget for a few cases, REPCORE achieves more stable improvements as  $K$  increases, suggesting that the continuous embedding geometry captures fine-grained inter-item relations that binary outcome vectors fail to preserve, thereby enabling more reliable and transferable coresets selection.

### C.4. Detailed Results on Source Model Quantity

In this section, we provide a comprehensive breakdown of the analysis presented in Section 3. To rigorously evaluate the sensitivity of each method to the availability of source models, we vary the source pool size  $|\mathcal{S}| \in \{5, 10, 15, 20\}$  across the full spectrum of computational budgets  $K \in \{10, 20, 30, 40, 50\}$ . The detailed performance metrics for each budget setting are reported in Tables 13 through 17.

The results consistently demonstrate the robustness of REPCORE in source-scARCe regimes. As evidenced across all budget levels, output-based baselines such as ANCHORPOINTS exhibit sharp performance degradation when  $|\mathcal{S}| = 5$ , suggesting a

heavy reliance on extensive statistical sampling to estimate item difficulty. In contrast, REP CORE maintains high ranking correlations even with minimal supervision, validating our hypothesis that the geometric structure of the representation space can be effectively aligned with limited source signals. Furthermore, performance saturation is observed as  $|\mathcal{S}|$  approaches 20, indicating that our framework captures the essential topology of the item space early, thereby eliminating the need for prohibitive data collection.

Table 13. Detailed results with budget  $K = 10$  under varying source pool sizes  $|\mathcal{S}|$ . We report Spearman’s rank correlation ( $\rho$ ,  $\uparrow$ ) and Mean Absolute Error (MAE,  $\downarrow$ ). **Bold** and underlined values denote the best and second-best results, respectively.

Method	ARC-C		BBH		GSM8K		SeedBench		MMLU-Pro	
	$\rho \uparrow$	MAE $\downarrow$								
$ \mathcal{S}  = 5$										
ANCHORPOINTS	<u>0.632</u>	0.216	0.614	0.176	0.714	0.210	0.513	0.228	0.673	0.187
GP-IRT	0.609	<u>0.088</u>	0.639	<u>0.106</u>	0.729	<u>0.079</u>	0.581	<u>0.095</u>	0.703	0.115
REP CORE	<b>0.704</b>	<b>0.077</b>	<b>0.706</b>	<b>0.104</b>	<b>0.749</b>	<b>0.074</b>	<b>0.590</b>	<b>0.088</b>	<b>0.744</b>	<b>0.096</b>
$ \mathcal{S}  = 10$										
ANCHORPOINTS	<b>0.724</b>	0.132	<u>0.701</u>	0.127	0.739	0.133	<b>0.653</b>	0.139	<b>0.754</b>	0.140
GP-IRT	0.706	<u>0.076</u>	0.681	<b>0.093</b>	0.750	<b>0.069</b>	0.594	0.098	0.646	0.101
REP CORE	<u>0.707</u>	<b>0.072</b>	<b>0.718</b>	<u>0.095</u>	<b>0.763</b>	<u>0.071</u>	0.642	<b>0.084</b>	0.732	<b>0.091</b>
$ \mathcal{S}  = 15$										
ANCHORPOINTS	0.562	0.126	<b>0.765</b>	0.117	<b>0.784</b>	0.110	<b>0.715</b>	0.123	<b>0.798</b>	0.128
GP-IRT	<b>0.719</b>	<u>0.081</u>	0.674	<b>0.090</b>	0.734	0.073	0.607	<u>0.092</u>	0.612	0.098
REP CORE	<u>0.699</u>	<b>0.074</b>	0.672	<u>0.098</u>	0.763	<b>0.070</b>	0.619	<b>0.091</b>	0.687	<b>0.095</b>
$ \mathcal{S}  = 20$										
ANCHORPOINTS	<b>0.683</b>	0.106	<b>0.787</b>	0.115	<u>0.762</u>	0.098	<b>0.737</b>	0.124	<b>0.809</b>	0.121
GP-IRT	0.638	<u>0.082</u>	0.620	<b>0.096</b>	0.711	<u>0.070</u>	0.616	<u>0.091</u>	0.566	0.106
REP CORE	<u>0.671</u>	<b>0.074</b>	0.717	<u>0.099</u>	<b>0.787</b>	<b>0.065</b>	0.638	<b>0.086</b>	0.682	<b>0.093</b>

### C.5. Detailed Results of Source Composition Ablation

In this section, we provide the detailed breakdown of the source model composition ablation study across five datasets: ARC-Challenge, BBH, GSM8K, SeedBench, and MMLU-Pro. Table 18 presents the Ranking Correlation (Spearman  $\rho$ ) and Estimation Error (MAE) for varying source pool sizes ( $N = \{10, 20, 30, 40, 50\}$ ).

### C.6. Detailed Results on Source Capability Range

In this section, we present the complete experimental results analyzing the impact of source model capability on compression performance. Table 19 provides a dataset-wise breakdown of the Ranking Correlation (Spearman  $\rho$ ) and Estimation Error (MAE) across varying source pool sizes ( $N = \{10, 20, 30, 40, 50\}$ ).

We compare three distinct source composition strategies:

- **Strong:** Pools consisting exclusively of the top-10 strongest models.
- **Weak:** Pools consisting exclusively of the bottom-10 weakest models.
- **Diverse (Ours):** A heterogeneous mix spanning the full capability spectrum.

The detailed results reaffirm the analysis in the main text: The **Diverse** strategy consistently achieves the best trade-off between ranking accuracy and estimation stability across all five datasets.

### C.7. Detailed Results on Coreset Size Generalization

In this section, we provide the comprehensive numerical results for the coreset size generalization experiments. We evaluate the robustness of different selection methods across three coreset sizes (100, 150, and 200 points). Table 20 presents the detailed breakdown, with Panel A showing the Spearman’s rank correlation coefficients ( $\rho$ ) and Panel B showing the Mean Absolute Error (MAE) on five benchmarks.

Table 14. Detailed results with budget  $K = 20$  under varying source pool sizes  $|\mathcal{S}|$ . We report Spearman’s rank correlation ( $\rho, \uparrow$ ) and Mean Absolute Error (MAE,  $\downarrow$ ). **Bold** and underlined values denote the best and second-best results, respectively.

Method	ARC-C		BBH		GSM8K		SeedBench		MMLU-Pro	
	$\rho \uparrow$	MAE $\downarrow$								
$ \mathcal{S}  = 5$										
ANCHORPOINTS	0.647	0.260	0.619	0.156	0.722	0.230	0.539	0.220	0.678	0.172
GP-IRT	<u>0.726</u>	<u>0.077</u>	<u>0.730</u>	<u>0.078</u>	<u>0.820</u>	<u>0.053</u>	<u>0.683</u>	<u>0.071</u>	<u>0.808</u>	<b>0.067</b>
REPCORE	<b>0.818</b>	<b>0.053</b>	<b>0.808</b>	<b>0.075</b>	<b>0.845</b>	<b>0.051</b>	<b>0.731</b>	<b>0.065</b>	<b>0.830</b>	0.069
$ \mathcal{S}  = 10$										
ANCHORPOINTS	0.767	0.136	<u>0.799</u>	0.097	0.794	0.132	<u>0.741</u>	0.119	0.800	0.107
GP-IRT	<u>0.808</u>	<u>0.057</u>	0.786	<b>0.068</b>	<u>0.839</u>	<u>0.057</u>	0.699	<u>0.063</u>	0.806	<b>0.065</b>
REPCORE	<b>0.820</b>	<b>0.050</b>	<b>0.824</b>	<u>0.069</u>	<b>0.872</b>	<b>0.047</b>	<b>0.755</b>	<b>0.060</b>	<b>0.829</b>	0.067
$ \mathcal{S}  = 15$										
ANCHORPOINTS	0.813	0.107	<b>0.840</b>	0.086	0.846	0.102	<b>0.796</b>	0.096	<b>0.848</b>	0.094
GP-IRT	<b>0.826</b>	<u>0.054</u>	0.779	<b>0.068</b>	0.828	0.051	0.719	<b>0.061</b>	0.755	0.069
REPCORE	<u>0.822</u>	<b>0.051</b>	<u>0.807</u>	<u>0.072</u>	<b>0.856</b>	<b>0.050</b>	0.713	<u>0.063</u>	<u>0.838</u>	<b>0.067</b>
$ \mathcal{S}  = 20$										
ANCHORPOINTS	<u>0.817</u>	0.092	<b>0.861</b>	0.084	0.831	0.088	<b>0.820</b>	0.092	<b>0.861</b>	0.088
GP-IRT	0.774	<u>0.055</u>	0.775	<b>0.067</b>	<u>0.842</u>	<b>0.049</b>	0.716	<b>0.059</b>	0.687	<u>0.078</u>
REPCORE	<b>0.823</b>	<b>0.051</b>	0.844	<u>0.071</u>	<b>0.870</b>	<u>0.051</u>	0.743	0.061	0.827	<b>0.065</b>

Table 15. Detailed results with budget  $K = 30$  under varying source pool sizes  $|\mathcal{S}|$ . We report Spearman’s rank correlation ( $\rho, \uparrow$ ) and Mean Absolute Error (MAE,  $\downarrow$ ). **Bold** and underlined values denote the best and second-best results, respectively.

Method	ARC-C		BBH		GSM8K		SeedBench		MMLU-Pro	
	$\rho \uparrow$	MAE $\downarrow$								
$ \mathcal{S}  = 5$										
ANCHORPOINTS	0.656	0.259	0.627	0.155	0.718	0.260	0.535	0.212	0.664	0.163
GP-IRT	<u>0.813</u>	<u>0.068</u>	<u>0.806</u>	<u>0.062</u>	<u>0.864</u>	<b>0.042</b>	<u>0.774</u>	<u>0.055</u>	<u>0.853</u>	<b>0.057</b>
REPCORE	<b>0.868</b>	<b>0.044</b>	<b>0.860</b>	<b>0.060</b>	<b>0.900</b>	<u>0.044</u>	<b>0.790</b>	<b>0.053</b>	<b>0.882</b>	<b>0.057</b>
$ \mathcal{S}  = 10$										
ANCHORPOINTS	0.792	0.138	<u>0.835</u>	0.087	0.832	0.125	<u>0.794</u>	0.108	0.846	0.102
GP-IRT	<u>0.845</u>	<u>0.052</u>	0.832	<u>0.058</u>	<u>0.857</u>	<u>0.051</u>	<u>0.780</u>	<b>0.050</b>	0.866	<b>0.053</b>
REPCORE	<b>0.871</b>	<b>0.041</b>	<b>0.870</b>	<b>0.057</b>	<b>0.905</b>	<b>0.039</b>	<b>0.819</b>	<u>0.051</u>	<b>0.875</b>	0.055
$ \mathcal{S}  = 15$										
ANCHORPOINTS	0.822	0.104	<b>0.873</b>	0.076	<u>0.887</u>	0.098	<b>0.838</b>	0.085	0.873	0.084
GP-IRT	<b>0.877</b>	<b>0.040</b>	0.843	<b>0.056</b>	0.872	<u>0.043</u>	<u>0.787</u>	<b>0.048</b>	0.837	0.056
REPCORE	0.875	<u>0.041</u>	<u>0.857</u>	<u>0.058</u>	<b>0.898</b>	<b>0.041</b>	0.783	<u>0.052</u>	<b>0.886</b>	<b>0.054</b>
$ \mathcal{S}  = 20$										
ANCHORPOINTS	0.835	0.094	<b>0.886</b>	0.074	0.874	0.084	<b>0.864</b>	0.076	<b>0.889</b>	0.079
GP-IRT	0.833	<u>0.043</u>	0.858	<b>0.054</b>	<u>0.882</u>	<u>0.042</u>	0.768	<b>0.049</b>	0.798	0.063
REPCORE	<b>0.878</b>	<b>0.041</b>	0.880	<u>0.055</u>	<b>0.909</b>	<b>0.041</b>	0.799	0.050	0.880	<b>0.053</b>

Table 16. Detailed results with budget  $K = 40$  under varying source pool sizes  $|\mathcal{S}|$ . We report Spearman’s rank correlation ( $\rho, \uparrow$ ) and Mean Absolute Error (MAE,  $\downarrow$ ). **Bold** and underlined values denote the best and second-best results, respectively.

Method	ARC-C		BBH		GSM8K		SeedBench		MMLU-Pro	
	$\rho \uparrow$	MAE $\downarrow$								
$ \mathcal{S}  = 5$										
ANCHORPOINTS	0.650	0.269	0.618	<u>0.150</u>	0.714	0.227	0.539	<u>0.215</u>	0.413	0.182
GP-IRT	<u>0.817</u>	<u>0.058</u>	<u>0.853</u>	<b>0.054</b>	<u>0.892</u>	<b>0.037</b>	<u>0.829</u>	<b>0.047</b>	<u>0.885</u>	<b>0.050</b>
REPCORE	<b>0.894</b>	<u>0.039</u>	<b>0.887</b>	<b>0.054</b>	<u>0.922</u>	<u>0.040</u>	<b>0.834</b>	<b>0.047</b>	<b>0.906</b>	<u>0.051</u>
$ \mathcal{S}  = 10$										
ANCHORPOINTS	0.797	0.145	0.854	0.081	0.864	0.117	0.818	0.103	0.861	0.095
GP-IRT	<u>0.866</u>	<u>0.043</u>	<u>0.869</u>	<u>0.052</u>	<u>0.865</u>	<u>0.042</u>	<u>0.824</u>	<b>0.043</b>	<u>0.899</u>	<b>0.046</b>
REPCORE	<b>0.900</b>	<u>0.036</u>	<b>0.898</b>	<b>0.049</b>	<b>0.926</b>	<b>0.035</b>	<b>0.853</b>	<u>0.045</u>	<b>0.906</b>	<u>0.048</u>
$ \mathcal{S}  = 15$										
ANCHORPOINTS	0.843	0.102	<b>0.896</b>	0.068	<u>0.903</u>	0.090	<b>0.865</b>	0.082	0.894	0.081
GP-IRT	<u>0.901</u>	<b>0.035</b>	0.887	<b>0.047</b>	0.897	<b>0.036</b>	0.841	<b>0.041</b>	0.887	<b>0.046</b>
REPCORE	<b>0.903</b>	<u>0.036</u>	0.894	<u>0.050</u>	<b>0.922</b>	<b>0.036</b>	0.822	<u>0.045</u>	<b>0.908</b>	<u>0.047</u>
$ \mathcal{S}  = 20$										
ANCHORPOINTS	0.767	0.096	<u>0.906</u>	0.065	0.892	0.080	<b>0.883</b>	0.070	0.904	0.076
GP-IRT	<u>0.867</u>	<u>0.037</u>	0.894	<b>0.046</b>	<u>0.900</u>	<u>0.038</u>	0.813	<b>0.042</b>	0.864	<u>0.052</u>
REPCORE	<b>0.903</b>	<u>0.035</u>	<b>0.911</b>	<u>0.047</u>	<b>0.928</b>	<b>0.037</b>	<u>0.831</u>	<u>0.045</u>	<b>0.906</b>	<b>0.047</b>

Table 17. Detailed results with budget  $K = 50$  under varying source pool sizes  $|\mathcal{S}|$ . We report Spearman’s rank correlation ( $\rho, \uparrow$ ) and Mean Absolute Error (MAE,  $\downarrow$ ). **Bold** and underlined values denote the best and second-best results, respectively.

Method	ARC-C		BBH		GSM8K		SeedBench		MMLU-Pro	
	$\rho \uparrow$	MAE $\downarrow$								
$ \mathcal{S}  = 5$										
ANCHORPOINTS	0.636	0.255	0.622	0.151	0.718	0.246	0.498	0.215	0.647	0.162
GP-IRT	<u>0.819</u>	<u>0.047</u>	<u>0.880</u>	<b>0.049</b>	<u>0.913</u>	<b>0.032</b>	<b>0.863</b>	<b>0.042</b>	<u>0.906</u>	<b>0.045</b>
REPCORE	<b>0.917</b>	<u>0.035</u>	<b>0.903</b>	<u>0.050</u>	<b>0.936</b>	<u>0.036</u>	<b>0.863</b>	<u>0.043</u>	<b>0.922</b>	<u>0.046</u>
$ \mathcal{S}  = 10$										
ANCHORPOINTS	0.796	0.143	0.867	0.078	0.880	0.116	0.835	0.098	0.867	0.094
GP-IRT	<u>0.884</u>	<u>0.036</u>	<u>0.901</u>	<b>0.045</b>	0.896	<u>0.034</u>	<u>0.863</u>	<b>0.038</b>	0.920	<b>0.041</b>
REPCORE	<b>0.921</b>	<u>0.032</u>	<b>0.913</b>	<b>0.045</b>	<b>0.938</b>	<b>0.032</b>	<b>0.874</b>	<u>0.040</u>	<b>0.924</b>	<u>0.043</u>
$ \mathcal{S}  = 15$										
ANCHORPOINTS	0.830	0.118	<b>0.904</b>	0.065	0.913	0.089	<b>0.877</b>	0.078	0.906	0.079
GP-IRT	<u>0.919</u>	<b>0.030</b>	<b>0.911</b>	<b>0.042</b>	<u>0.916</u>	<b>0.031</b>	<u>0.870</u>	<b>0.037</b>	<u>0.912</u>	<b>0.041</b>
REPCORE	<b>0.921</b>	<u>0.032</u>	<b>0.911</b>	<u>0.045</u>	<b>0.936</b>	<u>0.032</u>	0.849	<u>0.041</u>	<b>0.926</b>	<u>0.042</u>
$ \mathcal{S}  = 20$										
ANCHORPOINTS	0.850	0.087	0.919	0.059	0.904	0.079	<b>0.893</b>	0.066	0.916	0.074
GP-IRT	<u>0.898</u>	<b>0.032</b>	0.915	<b>0.041</b>	<u>0.910</u>	<u>0.034</u>	0.852	<b>0.036</b>	0.896	<u>0.045</u>
REPCORE	<b>0.921</b>	<u>0.032</u>	<b>0.927</b>	<u>0.043</u>	<b>0.941</b>	<b>0.033</b>	<u>0.859</u>	<u>0.040</u>	<b>0.924</b>	<b>0.041</b>

Table 18. Detailed ablation study on source model composition across five datasets. We compare single model families (e.g., Qwen, Llama, Ovis, InternVL) against a **Diverse** source composition (Ours). We report Spearman’s rank correlation ( $\rho$ ,  $\uparrow$ ) and Mean Absolute Error (MAE,  $\downarrow$ ). **Bold** and underlined values denote the best and second-best results, respectively.

(a) ARC-Challenge

Source Pool	$\rho \uparrow$					$MAE \downarrow$				
	N=10	N=20	N=30	N=40	N=50	N=10	N=20	N=30	N=40	N=50
Qwen	0.658	0.800	0.853	0.888	0.908	0.081	<u>0.055</u>	<u>0.046</u>	<u>0.041</u>	0.037
Llama	<b>0.725</b>	<b>0.833</b>	<b>0.879</b>	<b>0.904</b>	<u>0.921</u>	<u>0.078</u>	0.056	0.047	0.042	0.038
Diverse (Ours)	<u>0.707</u>	<u>0.820</u>	<u>0.871</u>	<u>0.900</u>	<b>0.921</b>	<b>0.072</b>	<b>0.050</b>	<b>0.041</b>	<b>0.036</b>	<b>0.032</b>

(b) BBH

Source Pool	$\rho \uparrow$					$MAE \downarrow$				
	N=10	N=20	N=30	N=40	N=50	N=10	N=20	N=30	N=40	N=50
Qwen	0.651	0.759	0.814	0.842	0.862	0.119	0.085	0.068	0.060	0.054
Llama	<u>0.661</u>	<u>0.811</u>	<u>0.862</u>	<u>0.888</u>	<u>0.904</u>	<u>0.099</u>	<u>0.072</u>	<u>0.060</u>	<u>0.054</u>	<u>0.048</u>
Diverse (Ours)	<b>0.718</b>	<b>0.824</b>	<b>0.870</b>	<b>0.898</b>	<b>0.913</b>	<b>0.095</b>	<b>0.069</b>	<b>0.057</b>	<b>0.049</b>	<b>0.045</b>

(c) GSM8K

Source Pool	$\rho \uparrow$					$MAE \downarrow$				
	N=10	N=20	N=30	N=40	N=50	N=10	N=20	N=30	N=40	N=50
Qwen	0.739	0.832	0.885	0.913	0.928	0.090	<u>0.065</u>	<u>0.057</u>	<u>0.052</u>	0.048
Llama	<u>0.754</u>	<u>0.854</u>	<u>0.898</u>	<u>0.919</u>	<u>0.934</u>	<u>0.087</u>	0.067	0.060	0.054	0.050
Diverse (Ours)	<b>0.763</b>	<b>0.872</b>	<b>0.905</b>	<b>0.926</b>	<b>0.938</b>	<b>0.071</b>	<b>0.047</b>	<b>0.039</b>	<b>0.035</b>	<b>0.032</b>

(d) SeedBench

Source Pool	$\rho \uparrow$					$MAE \downarrow$				
	N=10	N=20	N=30	N=40	N=50	N=10	N=20	N=30	N=40	N=50
Ovis	0.597	<b>0.756</b>	<b>0.826</b>	<b>0.864</b>	<b>0.883</b>	<u>0.093</u>	<u>0.063</u>	<u>0.054</u>	<u>0.049</u>	0.045
InternVL	<u>0.618</u>	0.741	0.802	0.837	0.859	0.094	0.073	0.065	0.059	0.055
Diverse (Ours)	<b>0.642</b>	<u>0.755</u>	<u>0.819</u>	<u>0.853</u>	<u>0.874</u>	<b>0.084</b>	<b>0.060</b>	<b>0.051</b>	<b>0.045</b>	<b>0.040</b>

(e) MMLU-Pro

Source Pool	$\rho \uparrow$					$MAE \downarrow$				
	N=10	N=20	N=30	N=40	N=50	N=10	N=20	N=30	N=40	N=50
Qwen	0.703	0.816	0.860	0.888	0.903	0.101	0.074	0.059	0.052	0.047
Llama	<u>0.716</u>	<u>0.823</u>	<b>0.876</b>	<u>0.902</u>	<u>0.921</u>	<u>0.097</u>	<u>0.070</u>	<u>0.057</u>	<u>0.050</u>	<u>0.045</u>
Diverse (Ours)	<b>0.732</b>	<b>0.829</b>	<u>0.875</u>	<b>0.906</b>	<b>0.924</b>	<b>0.091</b>	<b>0.067</b>	<b>0.055</b>	<b>0.048</b>	<b>0.043</b>

Table 19. Detailed ablation study on source capability range across five datasets. We compare homogeneous source pools consisting of only **Strong** or **Weak** models against a **Diverse** source composition (Ours). We report Spearman’s rank correlation ( $\rho$ ,  $\uparrow$ ) and Mean Absolute Error (MAE,  $\downarrow$ ). **Bold** and underlined values denote the best and second-best results, respectively.

(a) ARC-Challenge

Source Pool	$\rho \uparrow$					$MAE \downarrow$				
	N=10	N=20	N=30	N=40	N=50	N=10	N=20	N=30	N=40	N=50
Strong	0.479	0.659	<u>0.785</u>	0.843	0.868	0.125	0.144	0.154	0.144	0.128
Weak	<u>0.536</u>	0.713	0.782	<u>0.844</u>	<u>0.873</u>	<u>0.092</u>	<u>0.055</u>	<u>0.043</u>	<u>0.037</u>	<b>0.032</b>
Diverse (Ours)	<b>0.707</b>	<b>0.820</b>	<b>0.871</b>	<b>0.900</b>	<b>0.921</b>	<b>0.072</b>	<b>0.050</b>	<b>0.041</b>	<b>0.036</b>	<u>0.032</u>

(b) BBH

Source Pool	$\rho \uparrow$					$MAE \downarrow$				
	N=10	N=20	N=30	N=40	N=50	N=10	N=20	N=30	N=40	N=50
Strong	0.502	0.705	0.770	0.785	0.823	0.148	0.116	0.073	0.066	0.062
Weak	<u>0.654</u>	<u>0.758</u>	<u>0.817</u>	<u>0.855</u>	<u>0.890</u>	<u>0.098</u>	<u>0.075</u>	<u>0.061</u>	<u>0.054</u>	<u>0.050</u>
Diverse (Ours)	<b>0.718</b>	<b>0.824</b>	<b>0.870</b>	<b>0.898</b>	<b>0.913</b>	<b>0.095</b>	<b>0.069</b>	<b>0.057</b>	<b>0.049</b>	<b>0.045</b>

(c) GSM8K

Source Pool	$\rho \uparrow$					$MAE \downarrow$				
	N=10	N=20	N=30	N=40	N=50	N=10	N=20	N=30	N=40	N=50
Strong	<u>0.718</u>	0.812	<u>0.858</u>	<u>0.888</u>	<u>0.908</u>	0.120	0.094	0.079	0.065	0.056
Weak	0.612	<u>0.817</u>	0.839	0.874	0.905	<u>0.074</u>	<u>0.049</u>	<u>0.040</u>	<b>0.035</b>	<b>0.030</b>
Diverse (Ours)	<b>0.763</b>	<b>0.872</b>	<b>0.905</b>	<b>0.926</b>	<b>0.938</b>	<b>0.071</b>	<b>0.047</b>	<b>0.039</b>	<u>0.035</u>	<u>0.032</u>

(d) SeedBench

Source Pool	$\rho \uparrow$					$MAE \downarrow$				
	N=10	N=20	N=30	N=40	N=50	N=10	N=20	N=30	N=40	N=50
Strong	0.626	0.694	<u>0.748</u>	<u>0.802</u>	<u>0.846</u>	<u>0.089</u>	<u>0.079</u>	0.073	0.063	0.057
Weak	<b>0.683</b>	<u>0.696</u>	0.741	0.793	0.833	0.114	0.083	<u>0.063</u>	<u>0.052</u>	<u>0.051</u>
Diverse (Ours)	<u>0.642</u>	<b>0.755</b>	<b>0.819</b>	<b>0.853</b>	<b>0.874</b>	<b>0.084</b>	<b>0.060</b>	<b>0.051</b>	<b>0.045</b>	<b>0.040</b>

(e) MMLU-Pro

Source Pool	$\rho \uparrow$					$MAE \downarrow$				
	N=10	N=20	N=30	N=40	N=50	N=10	N=20	N=30	N=40	N=50
Strong	0.482	0.544	0.728	0.776	0.800	<u>0.119</u>	0.094	0.079	0.081	0.070
Weak	<u>0.614</u>	<u>0.743</u>	<u>0.815</u>	<u>0.871</u>	<u>0.896</u>	0.119	<u>0.082</u>	<u>0.067</u>	<u>0.056</u>	<u>0.049</u>
Diverse (Ours)	<b>0.732</b>	<b>0.829</b>	<b>0.875</b>	<b>0.906</b>	<b>0.924</b>	<b>0.091</b>	<b>0.067</b>	<b>0.055</b>	<b>0.048</b>	<b>0.043</b>

Table 20. Detailed generalization results with varying coresets sizes. We report  $\rho$  (Spearman’s rank correlation) and MAE on five benchmarks. The best results are **bolded** and the second best are underlined.

SIZE	METHOD	ARC	BBH	GSM8K	MMLU	SEEDBENCH
<b>PANEL A: <math>\rho</math> (<math>\uparrow</math>)</b>						
100	RANDOM	0.953	<u>0.948</u>	<u>0.958</u>	0.953	0.921
	APW	0.791	0.883	0.838	0.881	0.770
	GP-IRT	<u>0.957</u>	<u>0.948</u>	0.955	<b>0.960</b>	<b>0.934</b>
	REPCORE	<b>0.960</b>	<b>0.954</b>	<b>0.967</b>	<u>0.959</u>	<u>0.928</u>
150	RANDOM	0.969	<u>0.964</u>	<u>0.972</u>	0.968	0.947
	APW	0.777	0.888	0.829	0.884	0.781
	GP-IRT	<u>0.972</u>	0.961	0.968	<b>0.972</b>	<b>0.957</b>
	REPCORE	<b>0.973</b>	<b>0.967</b>	<b>0.977</b>	0.971	0.948
200	RANDOM	0.977	<u>0.972</u>	<u>0.979</u>	0.975	<u>0.959</u>
	APW	0.784	0.890	0.824	0.887	0.796
	GP-IRT	<u>0.979</u>	0.969	0.973	<u>0.977</u>	<b>0.967</b>
	REPCORE	<b>0.981</b>	<b>0.973</b>	<b>0.982</b>	<b>0.978</b>	<u>0.959</u>
<b>PANEL B: MAE (<math>\downarrow</math>)</b>						
100	RANDOM	0.0267	0.0378	0.0261	0.0385	0.0377
	APW	0.1430	0.0716	0.1480	0.0885	0.1040
	GP-IRT	<u>0.0228</u>	<b>0.0318</b>	0.0237	<b>0.0282</b>	<b>0.0274</b>
	REPCORE	<b>0.0227</b>	0.0328	<b>0.0233</b>	0.0314	0.0288
150	RANDOM	0.0211	0.0306	<u>0.0206</u>	0.0312	0.0303
	APW	0.1350	0.0704	0.1460	0.0866	0.0953
	GP-IRT	<u>0.0202</u>	<u>0.0289</u>	0.0215	<b>0.0236</b>	<b>0.0222</b>
	REPCORE	<b>0.0189</b>	<b>0.0271</b>	<b>0.0194</b>	0.0261	0.0239
200	RANDOM	<u>0.0175</u>	0.0264	0.0176	0.0271	0.0255
	APW	0.1210	0.0685	0.1330	0.0855	0.0850
	GP-IRT	0.0189	0.0270	0.0204	<b>0.0213</b>	<b>0.0194</b>
	REPCORE	<b>0.0168</b>	<b>0.0239</b>	<b>0.0173</b>	0.0231	0.0216

### C.8. Robustness to Temporal Drift

In this section, we provide a detailed analysis of the model’s robustness against temporal distribution shifts. We evaluate the performance of REOCORE compared to baselines across varying temporal shifts (represented by steps  $T \in \{10, 20, 30, 40, 50\}$ ). The experiments are conducted on five benchmarks: ARC, BBH, GSM8K, MMLU Pro, and SeedBench. Table 21 summarizes the Spearman’s rank correlation ( $\rho$ ) and Mean Absolute Error (MAE) for each method.

### C.9. Stability Comparison: REP CORE vs. Baselines

In this section, we provide a detailed visualization of the performance stability across five benchmarks. To ensure visibility of the standard deviation, we present the results in two parts. The error bars represent the standard deviation across multiple runs. REP CORE (red star) consistently shows lower variance compared to baselines.

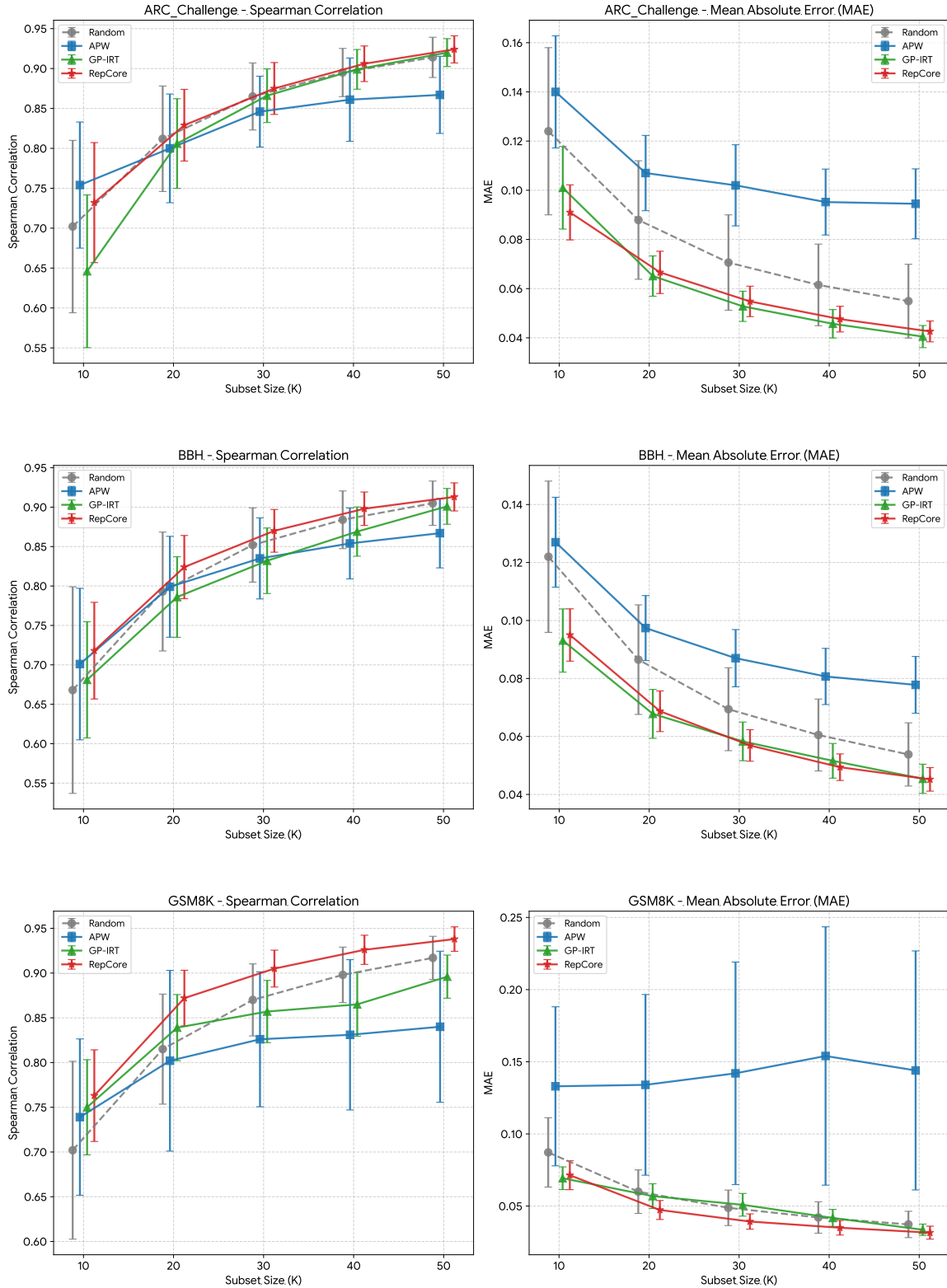
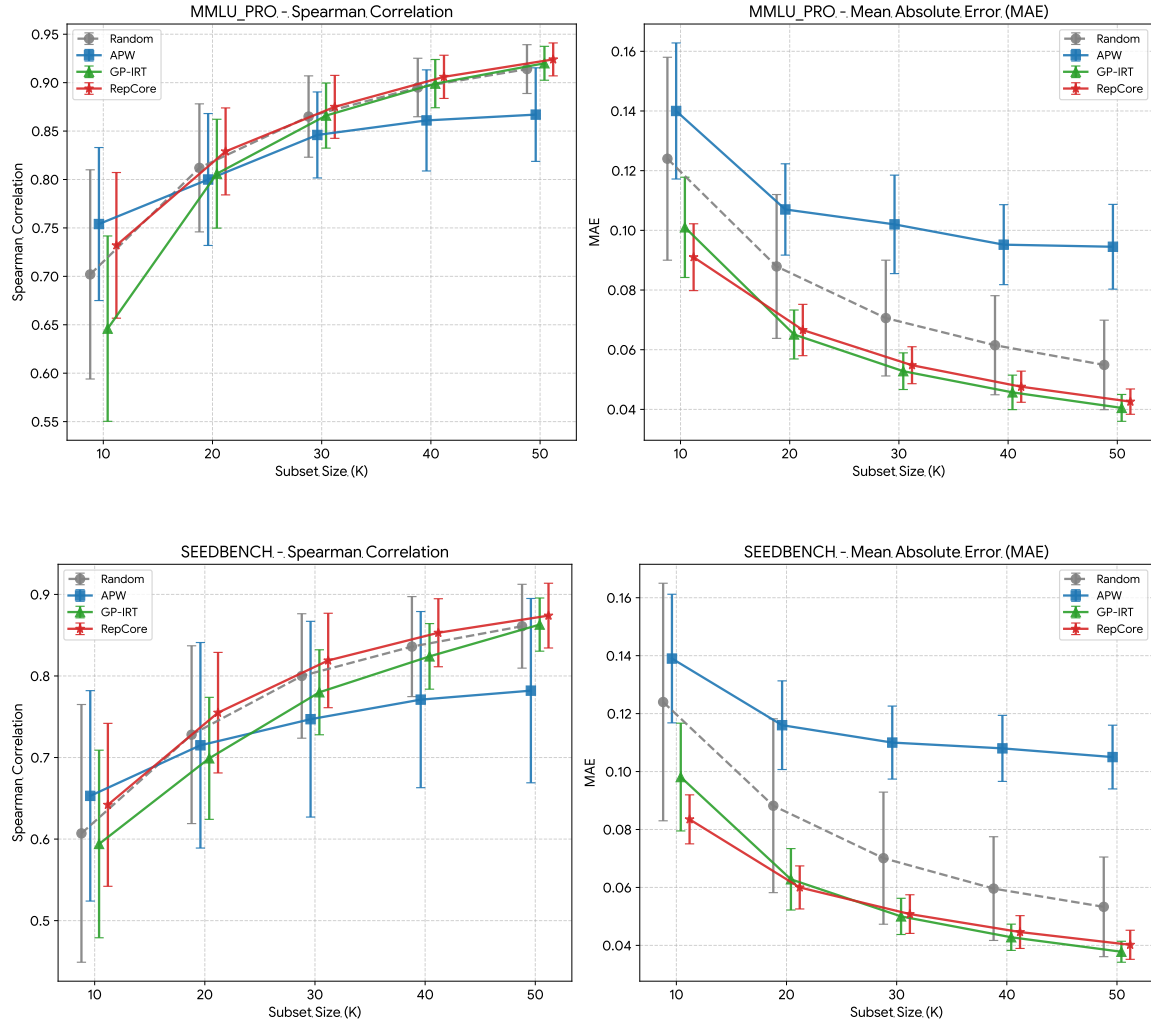


Figure 4. Stability Analysis (Part I): ARC, BBH, and GSM8K. The charts display Spearman Correlation (left) and MAE (right) with standard deviation error bars. Note the stability of REPCORE across varying coresets sizes.



**Figure 5. Stability Analysis (Part II): MMLU-PRO and SEEDBENCH.** Comparisons on larger-scale benchmarks similarly demonstrate the robustness of the proposed method.

Table 21. Detailed performance under temporal drift. We report  $\rho$  (Spearman's rank correlation) and MAE across different shift magnitudes (Steps 10-50). The best results are **bolded** and the second best are underlined.

STEP	METHOD	ARC	BBH	GSM8K	MMLU PRO	SEEDBENCH
<b>PANEL A: <math>\rho</math> (<math>\uparrow</math>)</b>						
10	RANDOM	0.676	0.706	0.714	<b>0.735</b>	0.555
	APW	<b>0.705</b>	0.716	0.758	0.707	<b>0.577</b>
	GP-IRT	<u>0.698</u>	0.704	0.724	<u>0.725</u>	0.549
	REOCORE	0.673	<b>0.719</b>	<b>0.772</b>	0.716	<u>0.574</u>
20	RANDOM	0.791	<u>0.817</u>	0.822	<b>0.842</b>	0.674
	APW	0.779	0.774	0.815	0.803	0.648
	GP-IRT	<b>0.822</b>	0.786	<u>0.826</u>	0.825	<b>0.679</b>
	REOCORE	<u>0.800</u>	<b>0.844</b>	<b>0.870</b>	0.831	0.666
30	RANDOM	0.848	<u>0.868</u>	<u>0.870</u>	<b>0.890</b>	<b>0.747</b>
	APW	0.806	0.819	0.838	0.830	0.691
	GP-IRT	<b>0.865</b>	0.845	0.863	0.870	0.733
	REOCORE	<u>0.861</u>	<b>0.885</b>	<b>0.908</b>	0.878	<u>0.735</u>
40	RANDOM	0.880	<u>0.896</u>	<u>0.898</u>	<b>0.912</b>	<b>0.792</b>
	APW	0.820	0.827	0.855	0.843	0.728
	GP-IRT	<u>0.886</u>	0.886	0.893	0.899	<u>0.791</u>
	REOCORE	<b>0.896</b>	<b>0.909</b>	<b>0.927</b>	0.905	0.779
50	RANDOM	0.901	<u>0.914</u>	<u>0.917</u>	<b>0.928</b>	0.820
	APW	0.820	<u>0.836</u>	<u>0.858</u>	0.867	0.772
	GP-IRT	<u>0.908</u>	0.906	0.916	0.922	<b>0.828</b>
	REOCORE	<b>0.914</b>	<b>0.920</b>	<b>0.942</b>	0.923	0.812
<b>PANEL B: MAE (<math>\downarrow</math>)</b>						
10	RANDOM	0.0832	0.1180	0.0833	0.1220	0.1180
	APW	0.1140	0.1400	0.1250	0.1420	0.1220
	GP-IRT	<b>0.0671</b>	<u>0.1060</u>	<b>0.0711</b>	<u>0.1030</u>	0.0934
	REOCORE	0.0742	<b>0.0994</b>	0.0724	<b>0.0993</b>	<b>0.0912</b>
20	RANDOM	0.0591	0.0837	0.0576	0.0865	0.0840
	APW	0.1100	0.1180	0.1250	0.1190	0.0992
	GP-IRT	<b>0.0476</b>	<b>0.0703</b>	<u>0.0519</u>	<u>0.0711</u>	<b>0.0614</b>
	REOCORE	0.0479	<u>0.0726</u>	<b>0.0516</b>	<b>0.0694</b>	0.0648
30	RANDOM	0.0484	0.0690	0.0469	0.0704	0.0671
	APW	0.1130	0.1070	0.1290	0.1120	0.0912
	GP-IRT	0.0398	<u>0.0592</u>	0.0434	<b>0.0565</b>	<b>0.0477</b>
	REOCORE	<b>0.0386</b>	<b>0.0581</b>	<b>0.0414</b>	0.0574	0.0525
40	RANDOM	0.0418	0.0587	0.0406	0.0610	0.0573
	APW	0.1130	0.1030	0.1270	0.1080	0.0863
	GP-IRT	<u>0.0352</u>	<b>0.0500</b>	<b>0.0357</b>	<b>0.0492</b>	<b>0.0400</b>
	REOCORE	<b>0.0325</b>	<u>0.0507</u>	<u>0.0366</u>	0.0498	0.0460
50	RANDOM	0.0368	0.0525	0.0356	0.0550	0.0537
	APW	0.1110	0.1000	0.1220	0.0945	0.0854
	GP-IRT	<u>0.0312</u>	<b>0.0441</b>	<b>0.0307</b>	<b>0.0429</b>	<b>0.0361</b>
	REOCORE	<b>0.0296</b>	<u>0.0461</u>	<u>0.0326</u>	0.0453	0.0411

Table 22. Models used for ARC Challenge benchmark.

Benchmark	Model Names
ARC Challenge	qwen2.5-72b-instruct, phi-4, qwen2.5-32b-instruct, llama-3.1-nemotron-70b-instruct-hf, llama-3.3-70b-instruct, qwen2.5-32b, deepseek-r1-distill-qwen-14b, qwen2-72b-instruct, qwen2.5-coder-32b-instruct, qwen2.5-14b-instruct-1m, dracarys-72b-instruct, qwen2.5-14b-instruct, qwen2.5-72b, aceinstruct-72b, smaug-llama-3-70b-instruct-32k, qwq-32b-preview, acemath-72b-instruct, qwen2.5-math-72b-instruct, yi-1.5-34b-chat, phi-3-medium-4k-instruct, yi-1.5-34b-chat-16k, dolphin-2.9.2-qwen2-72b, qwen2-math-72b-instruct, qwen2.5-14b, phi-3-medium-128k-instruct, qwen2.5-7b-instruct, qwen2.5-coder-14b-instruct, llama-3.1-tulu-3-70b-dpo, solar-pro-preview-instruct, hermes-3-llama-3.1-70b, llama-3.1-tulu-3-70b, aya-expans-32b, internlm2.5-20b-chat, aceinstruct-7b, llama-3.1-tulu-3-70b-sft, internlm2.5-7b-chat, phi-3.5-mini-instruct, dolphin-2.9.2-phi-3-medium-abliterated, mistral-small-instruct-2409, deephermes-3-mistral-24b-preview, dolphin-2.9.1-yi-1.5-34b, falcon3-7b-instruct, yi-1.5-9b-chat, llama-3.1-8b-instruct, yi-1.5-9b, dolphin3.0-r1-mistral-24b, yi-1.5-9b-chat-16k, dolphin-2.9.3-yi-1.5-34b-32k, qwen2.5-coder-7b-instruct, falcon3-10b-instruct, qwen2.5-3b-instruct, openchat-3.6-8b-20240522, qwen2-7b-instruct, dolphin-2.9.1-yi-1.5-9b, ministral-8b-instruct-2410, mistral-nemo-instruct-2407, acemath-7b-instruct, granite-3.1-8b-instruct, dolphin-2.9.3-mistral-nemo-12b, c4ai-command-r7b-12-2024, daredevil-8b-abliterated, llama-3-8b-sfr-iterative-dpo-r, meta-llama-3.1-8b-instruct-abliterated, aya-expans-8b, neuraledaredevil-8b-abliterated, hermes-3-llama-3.1-8b, granite-3.0-8b-instruct, granite-3.2-8b-instruct, qwen2.5-7b, llama-3.1-tulu-3-8b-dpo, aya-23-35b, llama-3.2-3b-instruct, llama-3.1-tulu-3-8b, yi-1.5-6b-chat, olmo-2-1124-7b-instruct, llama-3.1-tulu-3-8b-sft, mistral-7b-instruct-v0.3, dolphin-2.9.3-mistral-7b-32k, llama-3.1-8b-magpie-ultra, llama-3-refueled, dolphin3.0-llama3.1-8b, yi-1.5-34b, qwen2.5-math-7b-instruct, falcon-11b, yi-1.5-6b, falcon3-3b-instruct, yi-1.5-34b-32k, granite-3.2-2b-instruct, granite-3.1-2b-instruct, hermes-3-llama-3.2-3b, yi-1.5-9b-32k, codestral-22b-v0.1, aya-23-8b, granite-3.0-2b-instruct, qwen2-math-7b, openmath2-llama3.1-8b

## D. Model Pools for Each Benchmark

Tables provide comprehensive lists of models corresponding to each benchmark.

Table 23. Models used for BBH benchmark.

Benchmark	Model Names
BBH	phi-4, qwen2.5-72b-instruct, qwq-32b-preview, llama-3.3-70b-instruct, deepseek-r1-distill-llama-70b, llama-3.1-70b-instruct, qwen2.5-14b-instruct, qwen2.5-32b-instruct, llama-3.1-nemotron-70b-instruct-hf, acemath-72b-instruct, qwen2.5-coder-32b-instruct, deepseek-r1-distill-qwen-14b, deepseek-r1-distill-qwen-32b, qwen2.5-72b, smaug-llama-3-70b-instruct-32k, qwen2-72b-instruct, aceinstruct-72b, dracarys-72b-instruct, phi-3-medium-4k-instruct, qwen2.5-14b-instruct-1m, internlm2.5-20b-chat, qwen2.5-math-72b-instruct, dolphin-2.9.2-qwen2-72b, mistral-small-instruct-2409, phi-3-medium-128k-instruct, qwen2.5-coder-14b-instruct, dolphin3.0-r1-mistral-24b, qwen2-math-72b-instruct, internlm2.5-7b-chat, qwen2.5-7b-instruct, deephermes-3-mistral-24b-preview, gemma-2-27b-it, llama-3.1-tulu-3-70b-dpo, llama-3.1-tulu-3-70b, hermes-3-llama-3.1-70b, dolphin-2.9.1-yi-1.5-34b, yi-1.5-34b-chat, phi-3-small-128k-instruct, aya-expansse-32b, deepseek-r1-distill-qwen-7b, solar-pro-preview-instruct, llama-3.1-tulu-3-70b-sft, dolphin-2.9.2-phi-3-medium-abliterated, dolphin-2.9.3-yi-1.5-34b-32k, aceinstruct-7b, deepseek-r1-distill-llama-8b, llama-3.1-8b-instruct, phi-3-small-8k-instruct, mistral-nemo-instruct-2407, gemma-2-9b-it, qwen2.5-coder-7b-instruct, acemath-7b-instruct, codestr-22b-v0.1, granite-3.2-8b-instruct, granite-3.1-8b-instruct, ministr-8b-instruct-2410, falcon3-10b-instruct, yi-1.5-34b-chat-16k, phi-3.5-mini-instruct, llama-3-refueled, qwen2.5-7b, granite-3.0-8b-instruct, dolphin-2.9.3-mistral-nemo-12b, qwen2.5-14b, yi-1.5-34b-32k, qwen2-7b-instruct, aya-23-35b, yi-1.5-9b-chat, openchat-3.6-8b-20240522, llama-3-8b-sfr-iterative-dpo-r, qwen2.5-3b-instruct, hermes-3-llama-3.1-8b, k2-chat, daredevil-8b-abliterated, neuraldaredevil-8b-abliterated, falcon3-7b-instruct, llama-3.2-3b-instruct, dolphin-2.9.1-yi-1.5-9b, llama-3.1-tulu-3-8b-dpo, llama-3.1-tulu-3-8b, qwen2.5-math-7b-instruct, meta-llama-3.1-8b-instruct-abliterated, llama-3.1-tulu-3-8b-sft, openmath2-llama3.1-8b, llama-3.1-8b-magpie-ultra, yi-1.5-9b-chat-16k, dolphin-2.9.3-mistral-7b-32k, dolphin3.0-llama3.1-8b, yi-1.5-9b, aya-expansse-8b, yi-1.5-6b-chat, granite-3.0-8b-base, granite-3.0-2b-instruct, granite-3.2-2b-instruct, olmo-2-1124-7b-instruct, granite-3.1-8b-base, mistral-7b-instruct-v0.3, granite-3.1-2b-instruct, falcon3-3b-instruct, hermes-3-llama-3.2-3b, aya-23-8b

Table 24. Models used for GSM8K benchmark.

Benchmark	Model Names
GSM8K	acemath-72b-instruct, qwen2-math-72b-instruct, llama-3.3-70b-instruct, qwen3-30b-a3b, qwen2.5-72b-instruct, phi-4, qwq-32b-preview, qwen2.5-math-72b-instruct, qwen2.5-32b-instruct, llama-3.1-tulu-3-70b, llama-3.1-70b-instruct, qwen2.5-coder-32b-instruct, deepseek-r1-distill-qwen-14b, llama-3.1-tulu-3-70b-dpo, aceinstruct-72b, qwen2.5-14b-instruct, qwen2-72b-instruct, dracarys-72b-instruct, qwen2.5-14b-instruct-1m, hermes-3-llama-3.1-70b, smaug-llama-3-70b-instruct-32k, qwen2.5-72b, dolphin-2.9.2-qwen2-72b, qwen2.5-7b-instruct, deephermes-3-mistral-24b-preview, llama-3.1-tulu-3-70b-sft, mistral-small-instruct-2409, openmath2-llama3.1-8b, qwen2.5-32b, aceinstruct-7b, phi-3-medium-4k-instruct, llama-3.1-nemotron-70b-instruct-hf, yi-1.5-34b-chat, falcon3-7b-instruct, qwen2.5-14b, dolphin-2.9.2-phi-3-medium-abliterated, phi-3-medium-128k-instruct, deepseek-r1-distill-qwen-7b, gemma-2-9b-it, qwen2.5-coder-7b-instruct, llama-3.1-tulu-3-8b-dpo, ministr-8b-instruct-2410, aya-expansse-32b, dolphin-2.9.1-yi-1.5-34b, qwen2.5-7b, internlm2.5-20b-chat, phi-3.5-mini-instruct, llama-3.1-tulu-3-8b, acemath-7b-instruct, yi-1.5-9b-chat, llama-3.1-8b-instruct, deepseek-r1-distill-qwen-32b, granite-3.2-8b-instruct, mistral-nemo-instruct-2407, qwen2.5-math-7b, daredevil-8b-abliterated, qwen2.5-3b-instruct, dolphin-2.9.3-yi-1.5-34b-32k, dolphin-2.9.3-mistral-nemo-12b, neuraldaredevil-8b-abliterated, granite-3.1-8b-instruct, yi-1.5-9b-chat-16k, internlm2.5-7b-chat, hermes-3-llama-3.1-8b, olmo-2-1124-7b-instruct, qwen2-7b-instruct, llama-3.2-3b-instruct, openchat-3.6-8b-20240522, qwen2-math-7b, dolphin-2.9.1-yi-1.5-9b, deepseek-r1-distill-llama-70b, aya-expansse-8b, llama-3.1-tulu-3-8b-sft, dolphin-2.9.3-mistral-7b-32k, meta-llama-3.1-8b-instruct-abliterated, granite-3.0-8b-instruct, codestr-22b-v0.1, yi-1.5-6b-chat, falcon3-10b-instruct, granite-3.0-8b-base, granite-3.2-2b-instruct, granite-3.1-2b-instruct, llama-3-refueled, granite-3.0-2b-instruct, hermes-3-llama-3.2-3b, granite-3.1-8b-base, aya-23-35b, falcon3-3b-instruct, mistral-7b-instruct-v0.3, deepseek-r1-distill-llama-8b

Table 25. Models used for MMLU-Pro benchmark.

Benchmark	Model Names
MMLU-Pro	qwq-32b-preview, qwen2.5-72b-instruct, llama-3.3-70b-instruct, qwen2.5-32b-instruct, deepseek-r1-distill-qwen-14b, llama-3.1-nemotron-70b-instruct-hf, llama-3.1-70b-instruct, aceinstruct-72b, llama-3.1-tulu-3-70b-dpo, dracarys-72b-instruct, llama-3.1-tulu-3-70b, qwen2.5-14b-instruct, qwen2.5-14b-instruct-1m, qwen2.5-72b, qwen2.5-coder-32b-instruct, acemath-72b-instruct, qwen2.5-math-72b-instruct, qwen2.5-32b, solar-pro-preview-instruct, dolphin-2.9.2-qwen2-72b, smaug-llama-3-70b-instruct-32k, qwen2-math-72b-instruct, hermes-3-llama-3.1-70b, phi-3-medium-4k-instruct, qwen2.5-7b-instruct, deephermes-3-mistral-24b-preview, qwen2.5-coder-14b-instruct, phi-3-medium-128k-instruct, phi-3-small-128k-instruct, gemma-2-27b-it, llama-3.1-tulu-3-70b-sft, mistral-small-instruct-2409, aceinstruct-7b, dolphin-2.9.2-phi-3-medium-abliterated, phi-3-small-8k-instruct, yi-1.5-34b-chat, qwen2.5-14b, yi-1.5-34b-chat-16k, qwen2.5-7b, falcon3-7b-instruct, acemath-7b-instruct, gemma-2-9b-it, phi-3.5-mini-instruct, dolphin-2.9.1-yi-1.5-34b, aya-expanse-32b, qwen2.5-coder-7b-instruct, yi-1.5-9b-chat, qwen2-7b-instruct, mistral-nemo-instruct-2407, llama-3.1-tulu-3-8b-dpo, qwen2.5-3b-instruct, falcon3-10b-instruct, dolphin-2.9.3-yi-1.5-34b-32k, yi-1.5-9b-chat-16k, daredevil-8b-abliterated, llama-3.1-tulu-3-8b, ministral-8b-instruct-2410, dolphin-2.9.1-yi-1.5-9b, neuraldaredevil-8b-abliterated, llama-3.1-70b, yi-1.5-34b-32k, qwen2.5-math-7b-instruct, granite-3.2-8b-instruct, meta-llama-3.1-8b-instruct-abliterated, dolphin-2.9.3-mistral-nemo-12b, k2-chat, falcon3-3b-instruct, hermes-3-llama-3.1-8b, llama-3.1-tulu-3-8b-sft, llama-3-8b-sfr-iterative-dpo-r, yi-1.5-9b, yi-1.5-6b-chat, qwen2.5-math-7b, codestral-22b-v0.1, openchat-3.6-8b-20240522, dolphin3.0-llama3.1-8b, granite-3.0-8b-instruct, olmo-2-1124-7b-instruct, llama-3.1-8b-magpie-ultra, aya-23-35b, aya-expanse-8b, llama-3-refueled, mistral-7b-instruct-v0.3, qwen2-math-7b, granite-3.2-2b-instruct, granite-3.1-2b-instruct, yi-1.5-9b-32k, yi-1.5-6b, dolphin-2.9.3-mistral-7b-32k, granite-3.0-2b-instruct, hermes-3-llama-3.2-3b

Table 26. Models used for SEED-Bench-2-plus benchmark.

Benchmark	Model Names
SEED-Bench-2-plus	qwen2.5-vl-32b-instruct, internvl2.5-78b-mpo, qwen2.5-vl-72b-instruct, internvl3-78b, internvl3-38b, internvl2.5-38b-mpo, qwen2-vl-72b-instruct, ovis2-16b, ovis2-34b, mimo-vl-7b-rl, internvl2.5-78b, vARCo-vision-2.0-14b, internvl3-14b, internvl2.5-26b-mpo, wethink-qwen2.5vl-7b, internvl2.5-38b, internvl2-llama3-76b, ovis2-8b, internvl3-9b, qwen2.5-vl-7b-instruct, internvl2.5-26b, internvl2.5-8b-mpo, ovis-u1-3b, ovis2-4b, internvl2-40b, internvl3-8b, internvl2.5-8b, sail-vl-1d6-8b, ovis1.6-gemma2-9b, gemma-3-27b-it, sail-vl-1d5-8b, internvl2-8b-mpo, internvl2.5-4b-mpo, qwen2-vl-7b-instruct, internvl2-26b, gemma-3-12b-it, ovis2-2b, internvl2.5-4b, internvl-chat-v1-5, ristretto-3b, sail-vl-1d5-2b, points-qwen-2-5-7b-chat, internvl2-8b, qwen2.5-vl-3b-instruct, vARCo-vision-2.0-1.7b, ovis1.5-llama3-8b, llava-onevision-qwen2-7b-si-hf, llava-onevision-qwen2-7b-ov-hf, points-yi-1-5-9b-chat, phi-3-vision-128k-instruct, internvl2-4b, llama-3.2-11b-vision-instruct, xinyuan-vl-2b, qwen2-vl-2b-instruct, internvl3-2b, internvl2.5-2b-mpo, qtunenv1.5-2b, phi-3.5-vision-instruct, granite-vision-3.3-2b, gemma-3-4b-it, minicpm-llama3-v-2.5, granite-vision-3.2-2b, internvl2.5-2b, ovis2-1b, vintern-3b-beta, smolvlm2-2.2b-instruct, granite-vision-3.1-2b-preview, h2ovl-mississippi-2b, smolvlm-instruct, llama3-llava-next-8b-hf, mini-internvl-chat-4b-v1-5, internvl2.5-1b-mpo, mini-internvl-chat-2b-v1-5, llava-interleave-qwen-7b-hf, llava-interleave-qwen-7b-dpo-hf, molmo-7b-d-0924, internvl2-2b, qtunenv1.5-3b, molmo-7b-o-0924, pixtral-12b, llava-onevision-qwen2-0.5b-ov-hf, internvl2.5-1b, internvl2-1b, phi-4-multimodal-instruct, llama-1.5-13b-hf, smolvlm-synthetic, vintern-1b-v2, sharegpt4v-7b-hf, ovis1.6-llama3.2-3b, llava-onevision-qwen2-0.5b-si-hf, llava-1.5-7b-hf, minicpm-v, minicpm-v-2